Post-glacial sedimentary evolution and stratigraphy of the shallow offshore areas of the Shetland Islands (UK)

Rikza N.F. An Nahar[1,7*], Maarten Van Daele[1], Pedro J.M. Costa[2,3], Max Engel[4], Sue Dawson[5], Juliane Scheder[6], Thomas Goovaerts[6], Vanessa M.A. Heyvaert[6], and Marc De Batist[1]

- [1]Renard Centre of Marine Geology, Department of Geology, Ghent University, Ghent, Belgium (rikza.nahar@ugent.be) (maarten.vandaele@ugent.be) (marc.debatist@ugent.be)
- [2]Department of Earth Sciences, University of Coimbra, Coimbra, Portugal (ppcosta@dct.uc.pt)
- [3]Instituto Dom Luiz, Faculdade de Ciências da Universidade de Lisboa, Portugal (ppcosta@dct.uc.pt)
- [4]Institute of Geography, Heidelberg University, Heidelberg, Germany (max.engel@uni-heidelberg.de)
- [5]Energy, Environment and Society, University of Dundee, Dundee, United Kingdom (s.dawson@dundee.ac.uk)
- [6]Geological Survey of Belgium, Royal Belgian Institute of Natural Sciences, Brussels, Belgium (jscheder@naturalsciences.be) (tgoovaerts@naturalsciences.be) (vanessa.heyvaert@ugent.be)
- [7]Faculty of Industrial Technology, Sumatera Institute of Technology, South Lampung, Indonesia (rikza.faqih@gl.itera.ac.id)

*Corresponding author. Address as above. Email: rikza.nahar@ugent.be

Abstract

We present a high-resolution seismic–sedimentological reconstruction of post-glacial sedimentation in three shallow offshore basins around the Shetland Islands (Dury Voe, Colgrave Sound/Basta Voe, and Yell Sound), based on integrated multibeam bathymetry, sub-bottom profiler data, and 77 vibrocores supported by radiocarbon dating.

Sediment distribution is strongly controlled by inherited bedrock morphology, with post-glacial deposits preferentially accumulating in overdeepened sub-basins, while intervening highs remain sediment-starved. The stratigraphic successions consistently record four stages: (i) a pre-marine substrate of bedrock locally overlain by glacial or glaciofluvial deposits; (ii) early post-glacial infill formed under low-energy, restricted conditions (fluvial, lacustrine to estuarine/lagoonal); (iii) a transitional phase linked to early Holocene marine transgression and increasing hydrodynamic influence; and (iv) an upper unit dominated by sand-rich, current-influenced marine deposits forming laterally extensive mounded drift geometries.

High-amplitude, laterally continuous seismic units with sharp erosional bases and shell-rich, poorly sorted lithologies record regionally extensive extreme-wave events. Radiocarbon ages constrain the most prominent deposit to ca. 8.15 ka cal BP, enabling correlation with the Storegga Slide tsunami across offshore and nearshore settings. A younger event dated to ca. 1.5 ka cal BP is identified in Dury Voe and correlates with late Holocene onshore tsunami records in Shetland.

These results demonstrate that shallow voes preserve a coherent post-glacial stratigraphic framework, bridging offshore and onshore records, and provide new constraints on relative sea-level change and hydrodynamic reorganisation following marine transgression in formerly glaciated coastal systems.

Keywords: Post-glacial evolution, Seismic stratigraphy, Shallow offshore basins, Shetland Islands, extreme wave event deposit, Storegga

1 Introduction

Understanding offshore stratigraphy in shallow marine embayments is essential for reconstructing past environmental conditions and for establishing a robust geological framework of coastal systems. These environments often preserve continuous and relatively undisturbed sedimentary archives that reflect the interaction between marine and terrestrial processes and that are key to understanding long-term coastal evolution. The stratigraphic succession in such settings records the complex responses of coastal environments to external forcings, such as relative sea-level (RSL) fluctuations, which are in turn driven by both eustatic, isostatic and/or tectonic changes, sediment supply, and climatic variability (Gao and Collins, 2014; Hodgson et al., 2017).

The Shetland Islands represent the emergent part of a larger submerged platform composed of crystalline basement and volcanic and metasedimentary rocks, extending northeast from the British Isles and including mainland Scotland and Orkney (Mykura, 1976; Hall et al., 2021). During the Last Glacial Maximum (LGM), when global sea level was approximately 100–130 m lower than at present, the region was covered by the British–Irish Ice Sheet (BIIS). Following the collapse of the BIIS after the LGM, the Shetland Ice Cap developed as an independent ice mass before it collapsed and rapidly retreated as well (Clark et al., 2022). While the glacial history of the region has been increasingly well constrained by both onshore and offshore studies (Bradwell et al., 2019; Bradwell and Stoker, 2015; Hall et al., 2021; Phillips et al., 2008), the post-glacial sedimentary evolution of offshore basins and the development of coastal environments during the Holocene have received less attention so far. In particular, the relative roles of gradual processes such as RSL change and sediment supply, versus episodic high-energy events such as tsunamis, remain insufficiently understood in the offshore sedimentary record of the Shetland Islands.

To address these issues, studies involving shallow seismic surveying in combination with sediment coring are necessary. To date, however, only a limited number of investigations have focused on the nearshore stratigraphy of the Shetland Islands (Bradwell et al., 2019; Earland et al., 2024). The objective of this study is to elucidate the sedimentation history of this hitherto underexplored area through geophysical surveying and sediment coring. This involves reconstructing the stratigraphy based on sub-bottom profiler and multibeam bathymetry data and integrating them with sediment facies descriptions derived from core samples collected in a series of fjords (or voes, as they are locally called) and embayments around the Shetland Islands (Fig. 1). The findings hold significant value for understanding the dynamics of coastal evolution associated with the post-LGM marine transgression in the region and the interaction between long-term processes, such as RSL change and glacio-isostatic adjustment (Stockamp et al., 2015) and episodic high-energy events, including storms and tsunamis (Bondevik et al., 2005; Costa et al., 2021b; Dawson et al., 2006; Engel et al., 2024; Hess et al., 2024). These insights are expected to enhance our understanding of potential risks to infrastructure in shallow offshore areas of the Shetland Islands, contributing to improved risk assessment in the future.

2 Regional setting

2.1 Geological and Physiographic setting

The Shetlands, comprising over 100 islands, are situated in the North Sea to the northeast of mainland Scotland. They are underlain predominantly by metamorphic and metasedimentary rocks formed during the Caledonian Orogeny. These include schists, gneisses and quartzites belonging to the Dalradian Supergroup, which has experienced multiple deformation phases (Flinn, 2007; Mykura et al., 1976; Ritchie et al., 2011). The regional geological structure is strongly influenced by the Walls Boundary Fault, a major N–S-trending tectonic lineament that transects the Shetland Islands (Watts

et al., 2007). This structural framework controls the orientation and elongation of embayments and nearshore basins, which commonly align parallel to this fault system.

Surficial sediments on the shallow seafloor around Shetland are largely Holocene in age and exhibit a wide range of sediment types. The British Geological Survey classifies these sediments as muddy sand, sand, gravelly sand, and gravelly mud, reflecting a dynamic interplay of fluvial, tidal, and glacially derived inputs (British Geological Survey, 1991; Marine Scotland, 2019). These sediment types are particularly well-preserved in low-energy sub-basins formed between exposed bedrock highs (Fig. 1).

Three key areas were selected for focused investigation in this study: Yell Sound, Colgrave Sound/Basta Voe, and Dury Voe (Fig. 1). These areas were prioritized because of the presence of submarine basins suitable for offshore stratigraphic correlation, with sub-basins at different depths or gradual slopes that can potentially record sea level history, and because of the presence of tsunami deposits in adjacent onshore areas. At Basta Voe, a sand layer that was observed at several locations in coastal peat sections, has been interpreted as a tsunami deposit and dated to ca. 1500 cal BP (Bondevik et al., 2005; Dawson et al., 2006). At Ayre of Dury (Dury Voe), multiple peat exposures inland from the shoreline reveal a sand layer traceable up to 400 m inland, also dated to ca. 1500 cal BP (Bondevik et al., 2005). More recent chronological re-evaluation and synthesis of offshore and onshore records in Loch Flugarth suggest that this Late Holocene tsunami more likely occurred ca. 1400 cal BP (Engel et al., 2023) , highlighting uncertainties in earlier age constraints and the influence of reworked material on radiocarbon-based estimates. Additionally, sediments from Loch Garth, south of Dury Voe, contain evidence of a mid-Holocene tsunami event (i.e. the Garth tsunami), dated at ca. 5500 cal BP (Bondevik et al., 2005). In Sullom Voe (just south of Yell Sound), a sand layer preserved within peat deposits at an elevation of ca. 6 m above current high tide level has been dated to ca. 8150 cal BP, correlating with the Storegga Slide tsunami (Bondevik et al., 2003; Costa et al., 2021a; Dawson et al., 2020).

Beyond their scientific relevance, the Shetland voes and embayments are of economic and infrastructure importance. Hydrocarbon infrastructure, including oil and gas pipelines, cross the seabed at depths around 90 m as they enter Yell Sound, with shallower segments approaching critical nearshore facilities (Marine Scotland, 2019). Furthermore, the sheltered voes also support an extensive aquaculture industry, particularly fish catching, shellfish and salmon farming, which constitutes a major component of the regional economy (Shetland Islands Council, 2023). This adds further urgency to understanding sediment dynamics and geohazard potential in the region.

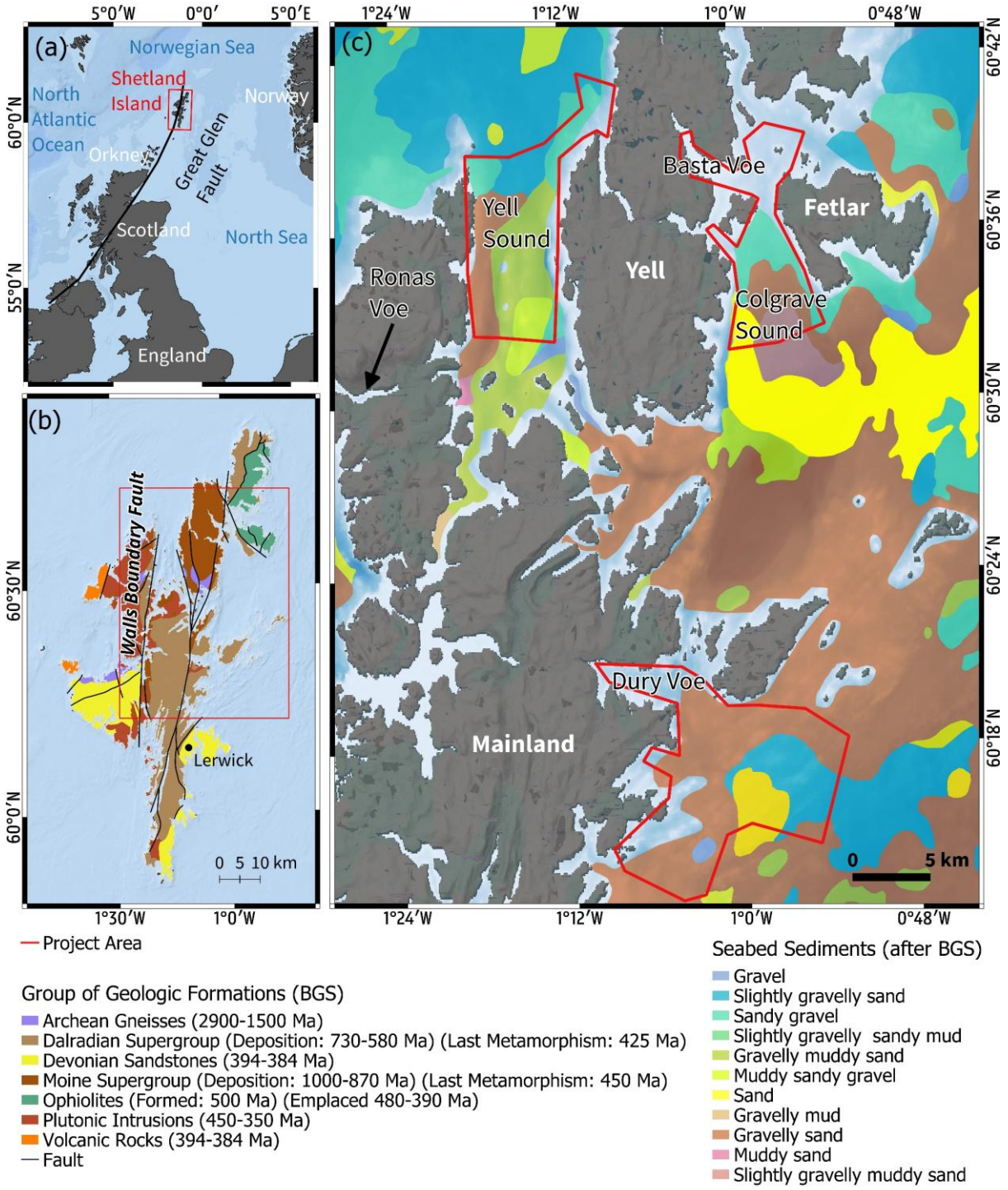

Figure 1. (a) Shetland Islands. (b) Geological map showing the main bedrock formations of the Shetland archipelago, including major fault zones (modified from Marine Scotland, 2019), study area indicated by red rectangle. (c) Seabed sediment distribution map based on data of the British Geological Survey (1991), displaying surface sediment types across the study area. Three survey areas of this study indicated by red polygons: Yell Sound, Colgrave Sound/Basta Voe, and Dury Voe. Sediment classification includes gravel, sand, mud, and mixed sediments. Background topography is derived from the SRTM digital elevation model (Farr et al., 2007).

2.2 Sea level changes and sediment dynamics

In the formerly glaciated Shetland Islands, post-glacial RSL history is complicated by glacio-isostatic adjustment and regional tectonic influences, resulting in a non-linear pattern of RSL change (Smith et al., 2019; Stockamp et al., 2015). These fluctuations critically influenced the development of

sedimentary environments from subaerially exposed surfaces to fully marine settings governing the distribution and preservation of depositional facies.

However, Holocene sea-level index points for Shetland remain sparse. The limited available data, derived primarily from basal peat deposits and a limiting marine shell from Ronas Voe, indicate that relative sea level was 10-15 m below present during the early Holocene and rose rapidly until approximately 7000–6000 yr BP, after which the rate of rise decreased markedly. Recent compilations of sea-level index points for Shetland suggest values of approximately −9 m around 6800–7800 yr BP and −2 m around 3500 yr BP, indicating a relatively limited range of Holocene RSL change compared to global trends (Shennan and Horton, 2002; Smith et al., 2019). These data imply that RSL remained below present prior to ca. 7 ka BP. Over the past ca. 1500 years, RSL change in Shetland appears to have been minimal (Shennan and Horton, 2002; Smith et al., 2019), consistent with tide-gauge observations from Lerwick showing negligible trends since the mid-20th century (Wahl et al., 2013).

Despite this, the semi-enclosed morphology of the voes provides favorable conditions for the preservation of sedimentary archives. Their restricted connection to the open coast promotes relatively continuous background sedimentation (Lo Giudice Cappelli et al., 2019). Superimposed on this background sedimentation, episodic high-energy events, such as storms and tsunamis, can locally generate erosion surfaces, sediment reworking, and event deposits within the stratigraphic sequence (Costa et al., 2021a; Dawson and Stewart, 2007). The sheltered voes also enhance the trapping and preservation of such event deposits, making these environments valuable archives for reconstructing past coastal hazards (Costa et al., 2021b; Costa and Andrade, 2020; Earland et al., 2024).

3 Methods and data

3.1 Acoustic imaging

Two surveys were conducted on board of RV Belgica (in December 2022 and September 2023), during which high-resolution geoacoustic data were acquired to image and characterize the stratigraphy in the shallow subsurface and to guide the selection of sites for sediment coring (Fig. 2). Sediment-filled depressions, incised valleys and depositional sinks were considered as high-priority targets. Sub-bottom data were acquired using a hull-mounted Kongsberg TOPAS PS18 parametric profiler aboard the RV Belgica. The system transmits two high-frequency signals that interact non-linearly in the water column to generate a secondary lower-frequency signal of 3.0 kHz, which provides a vertical resolution of ±15 cm. The ping interval was primarily set to 2 s and the trace length to 800 ms, but this was adjusted in real time based on seafloor conditions. A total of 212 seismic lines were collected, covering an accumulated survey track of 945 km (Costa et al., 2022; Van Daele et al., 2023).

During sub-bottom data acquisition, a Kongsberg EM2040 Multibeam Echosounder was operated in parallel to map seabed morphology. This system, optimized for shallow water applications, operated at 300 kHz with a maximum ping rate of 10 Hz. A swath angle of 10°/65° per transducer array was used in most areas, amounting to a total coverage of 130°. In shallower regions (<30 m), this was modified to 5°/70°, and increased further to 5°/75° on nearshore slopes during the second survey. Line planning followed best practices for bathymetric coverage, maintaining inter-line spacing of approximately three times the local water depth, as derived from hydrographic charts, to ensure sufficient overlap between adjacent swaths (Costa et al., 2022; Van Daele et al., 2023).

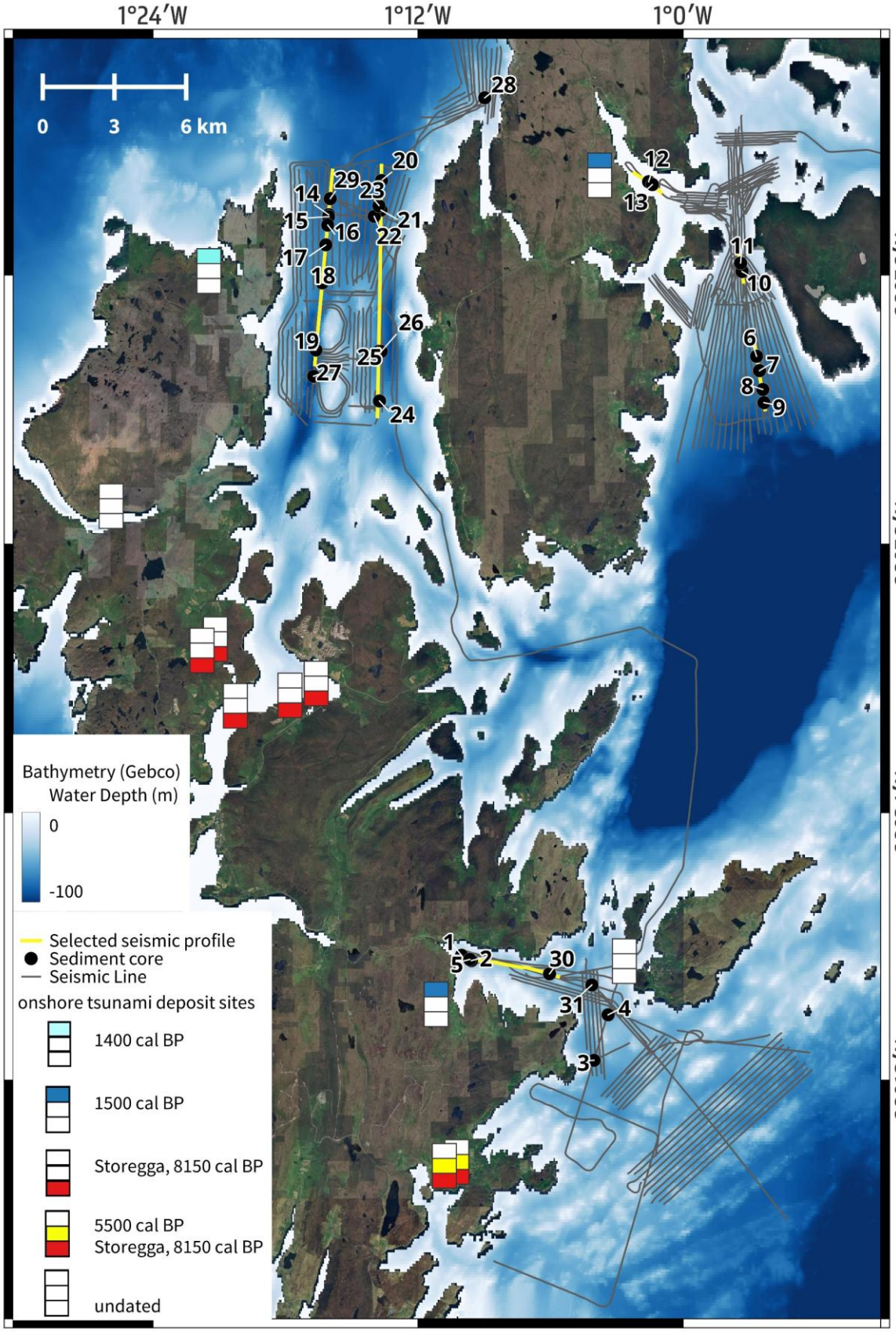

Figure 2. Map of the study areas: Yell Sound, Colgrave Sound/Basta Voe, and Dury Voe. Seismic lines, along which also multibeam echosounder bathymetry data were recorded, are marked as black lines. Seismic lines shown in Figs. 3, 6, 9, 10 are highlighted in yellow. A total of 31 vibrocoring sites are indicated by black dots. Onshore tsunami deposits are also shown in schematic boxes: light blue box (ca. 1400 cal BP event), dark blue box (ca. 1500 cal BP event), yellow box (5500 cal BP

event), red box (Storegga tsunami ca. 8150 cal BP), and no color boxes (undated). Bathymetric background data are derived from General Bathymetric Chart of the Oceans (GEBCO) 2025 grid with color gradients representing water depth (GEBCO Compilation Group, 2025).

3.2 Sediment coring: core collection and sedimentological analyses

During the second survey (September 2023), sediment cores were collected using a 4.5 m Ocean Scientific International Ltd. (OSIL) vibrocorer, which was provided and operated by the Flanders Marine Institute (VLIZ). The vibrocorer generates a vibrational force of up to 89 kN via electric motors, driving a barrel with a 9.6 cm diameter PVC liner into the seabed. Although the liners measured 4.5 m in length, the maximum sediment recovery was 3.5 m. This difference is due to factors such as sediment compaction, resistance during penetration, and equipment limitations, with additional material sometimes retained in the core catcher.

Coring sites were selected based on preliminary interpretation of the sub-bottom and bathymetric data, and positioning over the planned site was achieved through RV Belgica's DP2 dynamic positioning system. A total of 77 vibrocores were recovered from 31 sites across three study areas: Dury Voe (7 sites: SH23-01 to SH23-05, SH23-30, SH23-31), Colgrave Sound/Basta Voe (8 sites: SH23-06 to SH23-13) and Yell Sound (16 sites: SH23-14 to SH23-29) (Fig. 2) (Van Daele et al., 2023).

At each of the 31 coring sites, at least one core was taken (i.e. hole A). In addition, at most sites (27 sites) a duplicate core was retrieved from a second hole (i.e. hole B), located at a few meters from the initial hole A. At 19 sites also a triplicate core was recovered from a third hole (i.e. hole C). The A-cores were immediately sectioned onboard into segments of 1 m length, split longitudinally using a Geotek core splitter, and visually logged to describe lithostratigraphic units. This real-time assessment at the sampling site allowed for quick evaluation of stratigraphic patterns in the field, facilitating decisions on the necessity of B- and C-cores for undisturbed sampling. B-cores were split and described at the Renard Centre of Marine Geology, Ghent University. From all A- and B-cores high-resolution split-core surface images were acquired using a line-scan camera integrated into the Geotek Multi-Sensor Core Logger (MSCL). C-cores remained closed for optically-stimulated luminescence dating (not discussed in this manuscript, as analyses are still ongoing).

To supplement visual analysis, X-ray computed tomography (CT) scanning was performed on all (closed) B-cores, as well as (split) A-cores for which no B-core was available. Scans were acquired using a Siemens Definition Flash medical CT scanner at Ghent University Hospital and reconstructed to produce three-dimensional volumes with a voxel resolution of 0.2 × 0.2 × 0.3 mm, with the longest dimension oriented along the core's vertical axis. The CT data enabled detailed examination of internal sedimentary structures and supported stratigraphic interpretations, which were carried out using the Dragonfly software package.

3.3 Sediment coring: geochronology

To establish a chronological framework for the sedimentary sequences, radiocarbon dating was carried out on selected samples using accelerator mass spectrometry (AMS) at the Poznań Radiocarbon Laboratory, Poland (Goslar et al., 2004). A total of 16 samples were analyzed (Table 1), including five from Dury Voe, eleven from Colgrave Sound/Basta Voe and six from Yell Sound. Samples were selected based on the preservation and suitability of the material for accurate radiocarbon dating, primarily consisting of infaunal bivalve shells and terrestrially derived organic remains such as plant fragments. Sampling was conducted strategically across the core sections, targeting key lithologies, facies boundaries, and intervals indicative of depositional events. Additional samples were taken from background marine deposits and other stratigraphic intervals of paleoenvironmental significance to build a robust chronological framework. Articulated bivalves were identified on species level based on illustrations in Nolf and Vandenberge (2012a, 2012b) and Hayward and Ryland (2017)

Radiocarbon ages were calibrated using OxCal v4.3 (Bronk Ramsey, 1995). Marine samples (e.g., mollusk shells) were calibrated using the Marine20 calibration curve, while terrestrial samples (e.g.,

plant remains and peat) were calibrated using the IntCal20 calibration curve (Heaton et al., 2020; Reimer et al., 2020). All ages are reported in calibrated calendar years BP (before 1950 CE), based on the mean value of the 2σ calibrated age ranges. Due to the regional variability and unresolved magnitude of the marine reservoir effect in the northeastern Atlantic, particularly around Shetland, a ΔR value of -109 ±20 was applied to marine samples (Lo Giudice Cappelli and Austin, 2020; Earland et al., 2024; Reimer and Reimer, 2001).

Table 1. A table summarizing the radiocarbon sampling details for each site, including core sediment depths, sampled materials, and the estimated ages obtained.

Area	Core	Sample depth (cm)	Material	Lab Code Poznan	Radiocarbon age (yr BP)	Error (±1σ)	Calibrated age range (cal BP, 2σ)	Calibration curve
Dury Voe	SH23-01B	12.5	Articulated bivalve: *Thyasira flexuosa*	178553	105.67	0.3	Modern	Marine20
	SH23-02B	244	Shells from contact unit: gastropod shell	178522	9070	40	10333—10176	Marine20
	SH23-05B	10	Articulated bivalve: *Dosinia exoleta*	178454	425	30	Modern	Marine20
	SH23-05B	17.5	Articulated bivalve: Thyasira flexuosa	178455	465	30	Modern	Marine20
	SH23-05B	17.5	Bulk-organic sediment	178031	1590	30	1532—1403	Marine20
	SH23-05B	29.5	Articulated bivalve: *Nucula nucleus*	178456	425	30	Modern	Marine20
	SH23-05B	29.5	Bulk-organics sediment	178797	1370	30	1346—1178	Marine20
	SH23-05B	249	Articulated bivalve: *Abra alba*	178519	7330	50	8311—8017	Marine20
Colgrave Sound/ Basta Voe	SH23-07B	123	Articulated bivalve: *Dosinia exoleta*	178521	7750	50	8627—8417	Marine20
	SH23-09B	204	Articulated bivalve: *Mya truncata*	178520	11,820	60	13794—13513	Marine20
	SH23-12B	167	Wood	178798	8500	40	9542—9459	IntCal20
	SH23-12B	188	Wood	178800	7960	50	8991—8644	IntCal20
	SH23-12B	189	Wood	178819	8000	40	9007—8651	IntCal20
	SH23-12B	189	Unspecified plant remains	178820	8090	40	9251—8779	IntCal20
	SH23-13B	116.5	Unspecified plant remains (peat)	178821	9390	50	10750—10440	IntCal20
	SH23-13B	124.5	Unspecified plant remains (peat)	178822	9290	70	10658—10253	IntCal20
Yell Sound	SH23-14B	116	Unspecified plant remains	194944	6910	50	7918—7623	IntCal20
	SH23-16B	30	Articulated bivalve: *Lucinoma borealis*	195825	6850	40	7783—7605	Marine20
	SH23-16B	35	Articulated bivalve: *Lucinoma borealis*	195826	6890	40	7833—7620	Marine20
	SH23-16B	133	Articulated bivalve: *Dosinia exoleta*	195828	8580	50	9677—9481	Marine20
	SH23-17B	166.5	Large gastropod*: Aporrhais cf. Pespelecani*	195829	5860	35	6782—6561	Marine20
	SH23-29B	122.5	Articulated bivalve: *Lucinoma borealis*	195830	4150	35	4828–-4535	Marine20

3.4 Core-to-seismic correlation

To integrate the lithological and geochronological data from the sediment cores with information on lateral extent and variability in thickness, a core-to-seismic correlation was performed. Cores were first reconstructed to their original lengths (i.e. the original penetration depth below the seabed) to correct for incomplete recovery (as documented in RV Belgica Cruise Report 16/2023; Van Daele et al., 2023). A compaction correction of 25% was applied to the recovered sediment lengths. Cores and lithostratigraphic units were then projected onto the sub-bottom profiles using a seismic velocity of 1600 m/s, a value considered as typical for unconsolidated, predominantly sandy marine deposits (Best et al., 2007; Chotiros, 2002; Hamilton, 1980) and guided by the bathymetry for those cores that were not located directly on the profile.

4 Results and Interpretation

Multibeam bathymetry and sub-bottom profiling reveal that the three study areas are characterized by a predominantly rugged seafloor, with widespread bedrock exposures and highly variable sediment cover. Penetration of the sub-bottom profiles ranges from near-zero in areas of exposed bedrock, to a maximum of 20 m in localized depositional basins and mounded depocenters.

4.1 Dury Voe

4.1.1 Morphology

The multibeam bathymetry of Dury Voe reveals water depths ranging from 30 m b.s.l. (below sea level) in the inner voe to more than 70 m b.s.l. toward the outer basin (Fig. 3a). The seabed consists of a series of depressions separated by intervening topographic highs. The depressions generally display a relatively flat seabed, whereas the intervening highs exhibit irregular morphology and locally expose bedrock.

4.1.2 Seismic stratigraphy

The 45 sub-bottom profiles that were collected in Dury Voe reveal that sediment accumulation is confined to the isolated, sediment-filled depressions (Fig. 3b, c). The sedimentary cover in the area is characterized by acoustically well-stratified units, marked by laterally continuous reflections with alternating high and low reflection amplitudes. Four distinct seismic units can be identified, each with a different seismic facies. They are discussed below in ascending stratigraphic order:

- Seismic unit DV-SU1 forms the acoustic basement, which is marked by an irregular, high-amplitude upper reflection and comprises chaotic, low-amplitude internal reflections fading downwards to near-complete transparency at a few ms TWTT (two-way travel time) below the top reflection. Sub-unit DV-SU1a occurs locally, directly above the upper surface of DV-SU1. It forms a thin, laterally discontinuous package characterized by chaotic to semi-chaotic high-amplitude reflections.
- DV-SU2 is best developed in the western sub-basins where it reaches a maximum thickness of ca. 3.5 ms TWTT. The unit infills basement depressions and displays low- to medium-amplitude, sub-parallel reflections that onlap laterally, in a ‘ponding’ geometry, against the irregular upper reflection of seismic units DV-SU1 or DV-SU1a. The thickness of DV-SU2 varies across the sub-basins, but outside the western area the unit is absent or much thinner.
- DV-SU3 reaches a maximum thickness of around 8 ms TWTT in the westernmost sub-basin but becomes highly variable in thickness in the other sub-basins. The unit comprises laterally extensive, medium- to high-amplitude continuous reflections and is characterized by a locally mounded geometry. Within DV-SU3, two distinctive high-amplitude intervals (HAI1 and HAI2) can be recognized, representing thin, isolated sedimentary bodies ranging from 0.5 to 1.25 ms TWTT in thickness and consisting of high-amplitude reflections with irregular geometry, variable lateral continuity, and locally disrupted internal reflection patterns.
- At the top of the sedimentary sequence lies seismic unit DV-SU4, which reaches an average thickness of around 0.5 ms TWTT, with slightly greater thicknesses in the westernmost sub-basin. The unit is present throughout the Dury Voe study area, and is characterized by very high-amplitude, slightly chaotic, laterally continuous reflections that correspond to the most recent sediments deposited directly below the modern sediment–water interface.

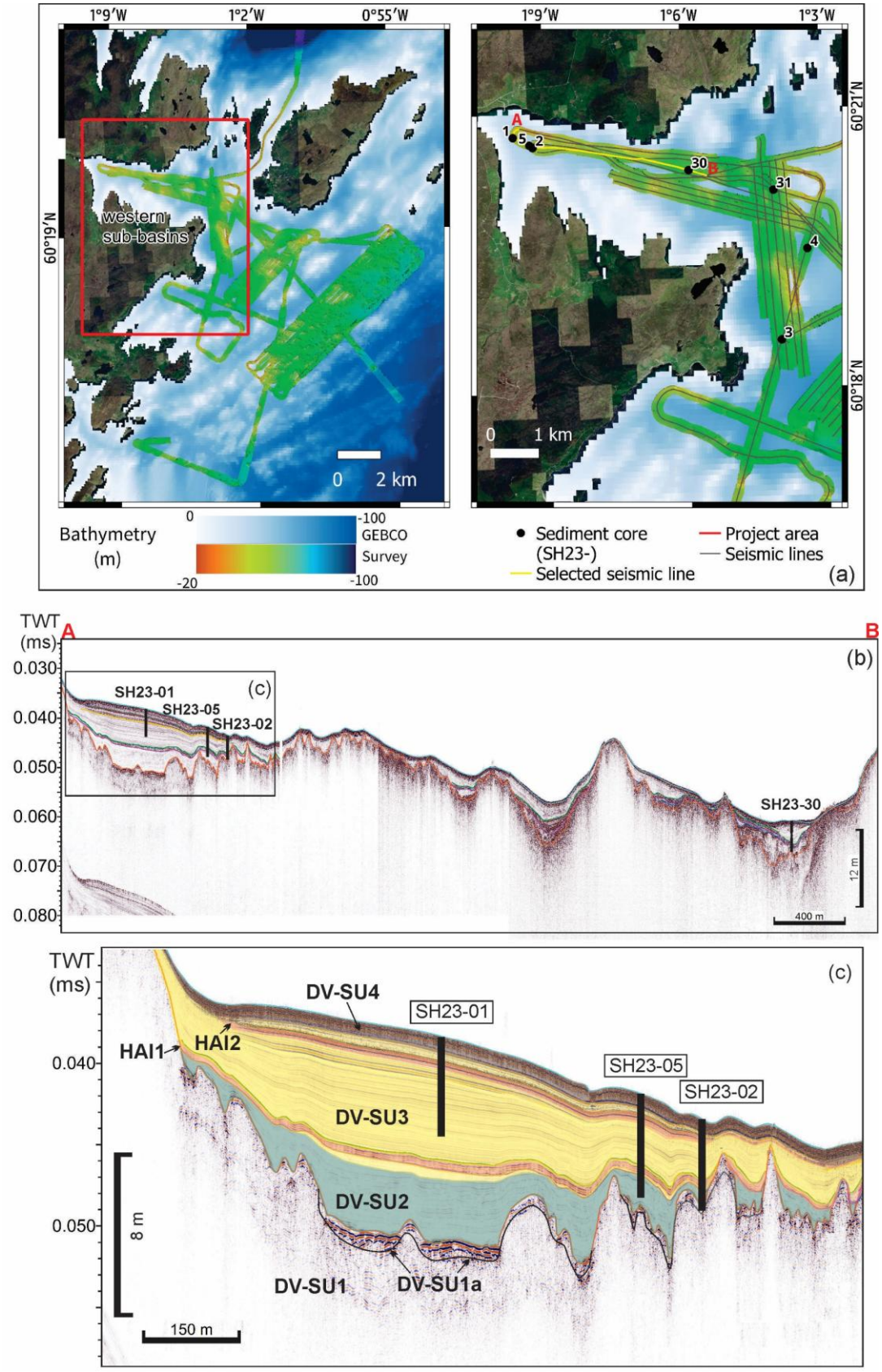

Figure 3. (a) Map showing the location of sub-bottom and multibeam bathymetry tracks, color-coded to illustrate the water depth (GEBCO Compilation Group, 2025). (b) Sub-bottom profile across the Dury Voe study area, highlighted in yellow (line A–B). (c) Interpreted sub-bottom profile from the western sub-basin in Dury Voe illustrating the different seismic units: DV-SU1 (uncolored), DV-SU2 (green), DV-SU3 (yellow) with HAI1 and HAI2 (dark yellow), and DV-SU4 (brown). Locations of coring sites are indicated.

4.1.3 Lithological units and core-to-seismic correlation

Vibrocores were collected at seven sites in Dury Voe (Fig. 3). In this section, we focus on four of these sites (SH23-01, SH23-02, SH23-05, and SH23-30), that are located along or close to the sub-bottom profile A-B in Fig. 3. Three of these sites (SH23-01, SH23-02, SH23-05) are located in the inner fjord, between 33.2 and 36.7 m b.s.l., whereas one site (SH23-30) is in the outer fjord at 50.0 m b.s.l. The remaining three cores were recovered from separate, smaller sub-basins within Dury Voe that are not intersected by the main seismic transect and display highly heterogeneous sedimentary successions dominated by shell hash and coarse deposits. These cores cannot be confidently tied to the seismic stratigraphy of the main basin but provide complementary information on local sediment variability.

Based on core lithology (including texture and sedimentary structures), high-resolution core photoscans and CT images, as well as thickness and nature of contacts with underlying and overlying deposits, five lithological units were identified in the Dury Voe cores (DV-LU1 to DV-LU5). They are described below in ascending stratigraphic order and can be correlated with the seismic stratigraphy of the basin (Fig. 4).

- Lithological unit DV-LU1 is the lowest lithological unit encountered in the cores at sites SH23-02 and SH23-30. It is a conglomerate with sub-angular pebbles of quartz and metamorphic rocks, up to 10 cm in diameter. It is clast-supported and the pebbles are embedded in a matrix of muddy sand. At site SH23-30 the conglomerate is overlain by coarse micaceous sand. This lithological unit corresponds to seismic sub-unit DV-SU1a observed on the sub-bottom profiles.
- DV-LU2 is the second lithological unit encountered at site SH23-30. It is characterized by sharp lithological contacts with the underlying (DV-LU1) and overlying (DV-LU4) units. It consists of poorly sorted coarse sand to fine gravel containing scattered (sub-)angular dark pebbles and displaying a dark-grey color. This unit likely represents the upper part of seismic unit DV-SU1.
- DV-LU3 is the lowest lithological unit encountered at site SH23-05, while at site SH23-02 it overlies DV-LU1. It consists of olive-green silty clay containing shell fragments up to 4 cm in size that occur throughout the unit. This lithological unit corresponds to seismic unit DV-SU2.
- DV-LU4 is a thick lithological unit that is present at all sites and that is characterized by sharp lithological contacts with the overlying (DV-LU5) and underlying units (DV-LU2 or DV-LU3). It mostly consists of medium- to dark-grey, well-sorted bioclastic sand containing minor shell fragments and rare coarser clasts. At site SH23-30, this lithological unit is generally coarser-grained than at the sites in the inner fjord. Two relatively thin interbeds (ca. 5 to 20 cm thick, but laterally variable) are embedded within DV-LU4. They consists of greyish olive-green, poorly sorted coarse sand with quartz grains, darker minerals, and abundant angular shell fragments. The lower interbed occurs ca. 20–30 cm above the base of DV-LU4 at sites SH23-05 and SH23-02, and ca. 10 cm above the base at site SH23-30, where it is subdivided into three separate packages. This interbed is slightly coarser-grained, both in the minerogenic and bioclastic fractions. The upper interbed occurs approximately 20–40 cm below the top of DV-LU4 at sites SH23-01, SH23-05 and SH23-02, and consists of a package with normal grading to the top of the layer. DV-LU4 corresponds to seismic unit DV-SU3, while the two coarse-grained interbeds correlate with the high-amplitude intervals (HAI1 and HAI2) identified on the seismic profiles.
- DV-LU5 represents the uppermost lithological unit in the cores of inner-voe sites SH23-01, SH23-05 and SH23-02. It consists of dark-brown, organic-rich, moderately sorted fine sand containing sparse shell fragments, which are slightly more abundant near the base of the unit. DV-LU5 is absent at the more easterly site SH23-30. This unit corresponds to seismic unit DV-SU4.

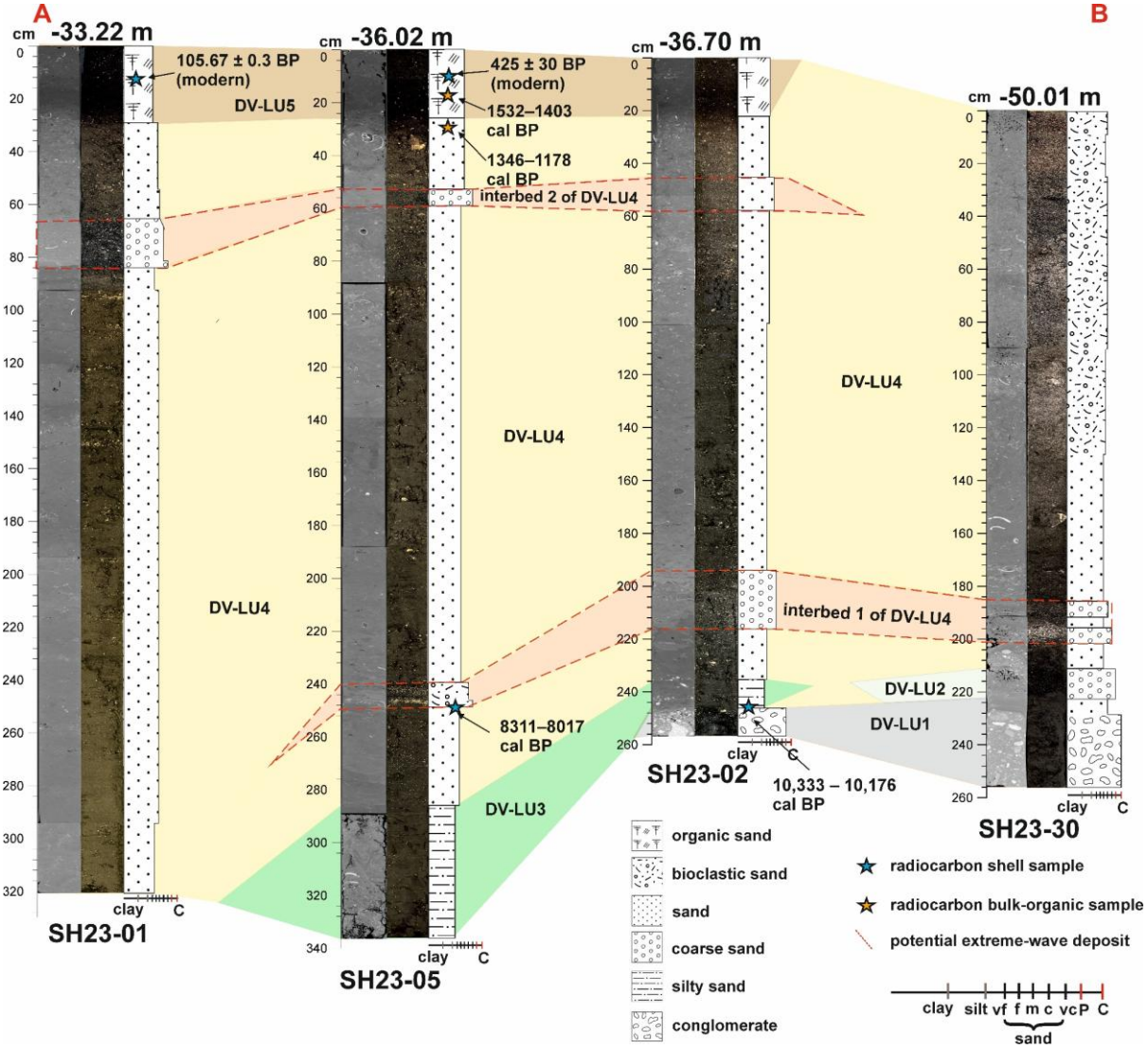

Figure 4. Core transect in Dury Voe (Fig. 3). Every core is shown with, from left to right, a high-resolution CT scan, a color-calibrated linescan image and a litholog, which is based on visual core description and interpretation. Shifts in vertical position of the cores along the transect highlight the differences in water depth at the core locations but are not to scale. Calibrated radiocarbon ages are indicated. Potential extreme-wave event deposits (?) are marked in orange with red dashed line.

4.2 Colgrave Sound/Basta Voe

4.2.1 Morphology

The multibeam bathymetry of Colgrave Sound/Basta Voe reveals water depths ranging from 15 to 30 m b.s.l. in the shallow northwestern sector (Basta Voe) to more than 80 m b.s.l. in the southern basin (part of Colgrave Sound) (Fig. 5). Colgrave Sound has a funnel-shaped morphology that is characterized by a deep, elongate depression in its southern part, which gradually shallows northward towards Yell Island. Across the sound, but more common in the shallower northern part, irregular topographic highs and ridges interrupt smoother lower-lying areas. The morphology in the shallower Basta Voe resembles that of Dury Voe, with the topographic highs dividing the voe in sub-basins, with a flat or locally mounded seafloor.

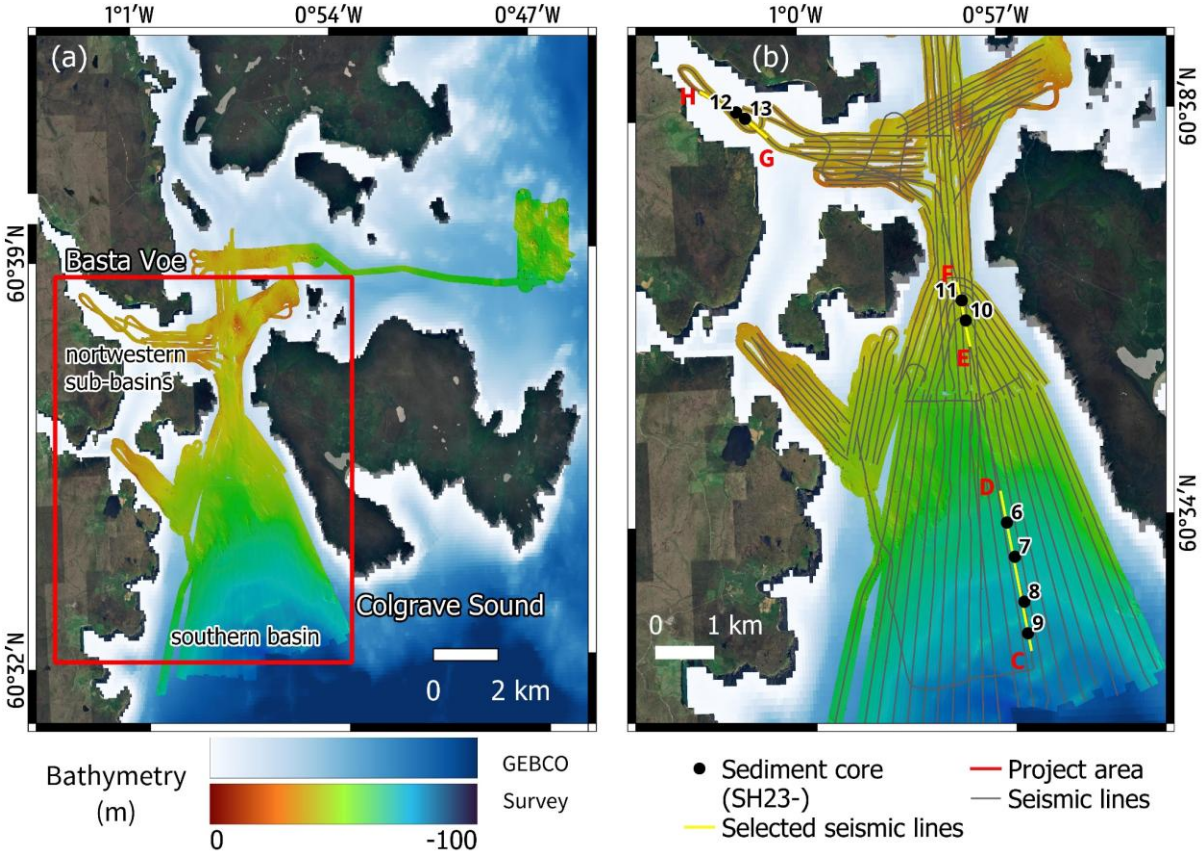

Figure 5. Bathymetric and seismic survey lines from Colgrave Sound/Basta Voe. (a) Multibeam bathymetry overlain on 2025 grid with color gradients representing water depth (GEBCO Compilation Group, 2025). (b) Sub-bottom seismic survey tracks (black lines) and sediment core locations within the project area. Seismic lines shown in Fig. 6 (C–D, E–F, and G–H), along which eight sediment cores were collected to ground-truth stratigraphic interpretations, are highlighted in yellow.

4.2.2 Seismic stratigraphy

The sub-bottom seismic profiles collected in Colgrave Sound/Basta Voe cover a total of 91 survey lines or 295 km of cumulative profile distance, extending from the deeper southern sector toward the shallower northern margin and the Yell shoreline (Fig. 5b). The seismic lines C–D, E–F, and G–H illustrate the stratigraphic configuration and show four distinct seismic units (CB-SU1 to CB-SU4)(Fig. 6):

- CB-SU1 forms the acoustic basement. It is characterized by chaotic, low-amplitude internal reflections that fade out downward from the irregular, high-amplitude upper boundary. The unit is discontinuous and displays strong relief with rugged local highs and depressions. Locally, sub-unit CB-SU1a occurs directly above the upper surface of CB-SU1. It forms a thin, laterally discontinuous package characterized by chaotic to semi-chaotic, low-amplitude reflections with no coherent internal layering. The sub-unit exhibits variable thickness of up to 3 ms TWT, infilling basement depressions and hummocks on top of highs. Its upper boundary is defined by a distinct but uneven reflection, while its lower boundary transitions into the underlying chaotic facies of CB-SU1.
- CB-SU2 overlies the acoustic basement and is mostly defined by low- to medium-amplitude reflections with variable internal continuity. The unit shows localized onlapping geometries against basement highs and preferentially infills depressions, producing a ponded geometry. Its seismic character varies between different basement depressions and water depths. In the southern deeper depressions (Colgrave Sound), CB-SU2 consists of packages with irregular to moderately continuous reflections, whereas in shallower regions (Basta Voe) the unit becomes thinner and

locally displays prograding clinoform geometries or chaotic, low-amplitude basin infills in localized depressions, such as in the area of site SH23-13. In the southern sector, CB-SU2 thickens to 12 ms TWT, while across intervening highs it is very thin or absent.

- CB-SU3 is a thin unit distinguished by high-amplitude, laterally continuous reflections with a sharp basal boundary. Internal reflections are parallel to sub-parallel. The unit locally thickens adjacent to bedrock highs and basin margins, attaining more than 2 ms TWT in places, but elsewhere thins to less than 1 ms.
- CB-SU4 is the uppermost stratigraphic unit and is characterized by predominantly low- to medium-amplitude, parallel internal reflections. The unit is laterally extensive across the voe and has a sharply defined upper boundary corresponding to the present seabed. CB-SU4 locally onlaps against steep bedrock highs but generally displays a less ponding and more draping geometry than the underlying units. The amplitude of internal reflections varies with water depth: reflections in the deeper parts of the system, particularly within Colgrave Sound, generally have a higher amplitude, whereas in the shallower areas, such as Basta Voe, they appear weaker. In several locations the unit forms strongly mounded accumulations, producing a locally asymmetric thickness pattern with maximum thickness of 12 ms. CB-SU4 typically attains up to 5 ms TWT in thickness.

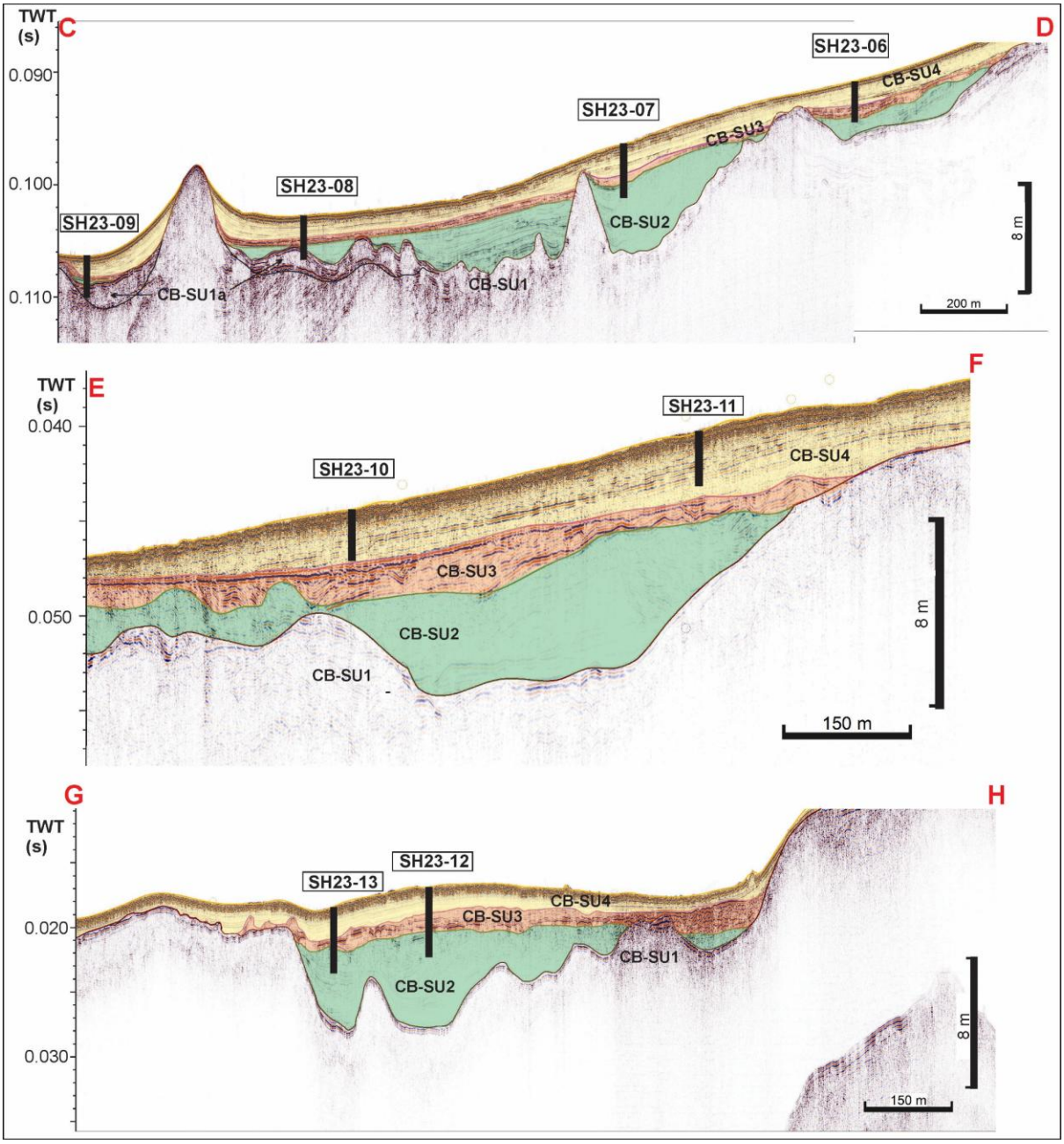

Figure 6. Sub-bottom profiles from Colgrave Sound/Basta Voe showing sediment stratigraphy from the deeper sub-basin (Colgrave Sound) to the shallower sub-basin (Basta Voe) (see Fig. 5b for exact location). Locations of coring sites (SH23-06 to SH23-13) are indicated. Interpreted versions of the profiles, illustrating four seismic units: CB-SU1 and CB-SU1a (no color), CB-SU2 (green), CB-SU3 (orange), and CB-SU4 (yellow).

4.2.3 Lithological units and core-to-seismic correlation

Vibrocores were collected from eight sites in different geomorphological settings within Colgrave Sound/Basta Voe (Fig. 5). Four sites (SH23-06, SH23-07, SH23-08, SH23-09) are located in the deeper southern basin of Colgrave Sound, at present-day water depths of 85.3 m, 82.0 m, 72.2 m and 71.0 m b.s.l., respectively. Two sites (SH23-10, SH23-11) are located in the northern part of Colgrave Sound, at water depths of 37.9 m and 34.8 m b.s.l., and two sites (SH23-12 and SH23-13) are located in Basta Voe, at depths of 25.5 m and 24.6 m b.s.l.

Based on core lithology, color-calibrated core imagery and CT scans, seven lithological units (CB-LU1 to CB-LU7) were identified and correlated with the seismic units recognized on the sub-bottom profiles (Fig. 6). They are described below in ascending stratigraphic order (Fig. 7):

- CB-LU1 is the lowest unit encountered in the cores at sites SH23-08 and SH23-09. It is a diamicton composed of a sandy silt matrix containing several clay-rich clasts and embedded sub-rounded quartz and metamorphic pebbles up to 8–10 cm in diameter. The unit is locally clast-supported and exhibits a massive structure with a sharp upper boundary. This unit corresponds to seismic sub-unit CB-SU1a, which represents the uppermost part of the acoustic basement.
- CB-LU2 is observed in cores from the shallower Basta Voe (sites SH23-12, SH23-13). It consists of fine to medium-grained micaceous sand, enriched in darker minerals. The unit is strongly stratified and displays horizontal bedding with parallel to wavy laminations. It can locally be subdivided into several sub-units: finer micaceous sandy intervals, darker mineral-rich sandy horizons, and coarser gravelly to very coarse sandy interbeds. At site SH23-12, organic-rich and peaty laminae are observed within the sub-units. Marine bioclasts are absent. This lithological unit corresponds to the more heterogeneous seismic facies of CB-SU2 observed in the shallower sector of the basin. The lithological variability likely corresponds to the prograding and heterogeneous seismic facies of CB-SU2 observed in this sector.
- CB-LU3 is present only at site SH23-13, located in a local depression in Basta Voe. The unit is ca. 10 cm thick and directly overlies CB-LU2. It consists of compact fibrous dark-brown peat with minor sandy interbeds and shows a sharp basal contact. This thin organic-rich unit corresponds to a local acoustic anomaly within the lower part of CB-SU3.
- CB-LU4 is present in the cores at the southern Colgrave Sound sites SH23-06, SH23-07, SH23-08, SH23-09 and locally in Basta Voe (site SH23-13). It consists of sandy silt at the bottom and gradually grades to fine sand with occasional marine shell fragments. The unit displays a dark grey to olive-grey color. Contacts with the underlying and overlying units are generally sharp. This lithology corresponds to the low- to medium-amplitude, weakly stratified seismic facies of CB-SU2 observed in the deeper southern basin.
- CB-LU5 overlies CB-LU4 in Colgrave Sound (sites SH23-06, SH23-07, SH23-08, SH23-09) and CB-LU4 and CB-LU2 in Basta Voe (sites SH23-12, SH23-13). The unit shows lateral variability in sedimentary structure and texture across the basin. However, it is sandy on all locations with a sharp and distinct basal contact. At several sites (e.g., SH23-12), CB-LU5 is laminated, consisting of alternating fine- to coarse-grained sandy layers, locally devoid of shell fragments. In contrast, at site SH23-13 the unit is massive and rich in coarse angular shell fragments, forming a poorly sorted, shell-bearing sand. At sites SH23-07 and SH23-06, CB-LU5 is subdivided into multiple sub-units distinguished by variations in grain size and the abundance of shell material. It corresponds to seismic unit CB-SU3, which is characterized by high-amplitude reflections on the sub-bottom profiles.
- CB-LU6 occurs at sites SH23-10 and SH23-11 in the central sector between Colgrave Sound and Basta Voe. It consists of bioclastic sand containing gravel-sized clasts rich in bryozoans and highly concentrated bivalve fragments. The unit displays a massive to chaotic structure with only minor minerogenic components, including dark sub-rounded pebbles up to 2 cm in length embedded within a sandy matrix.
- CB-LU7 represents the uppermost sedimentary unit in all coring sites. It consists of bioclastic medium- to coarse-grained sand rich in fragmented bivalves and other shell material. The unit is generally well sorted but locally contains coarser pockets and shell hash. Together, CB-LU6 and CB-LU7 correspond to seismic unit CB-SU4.

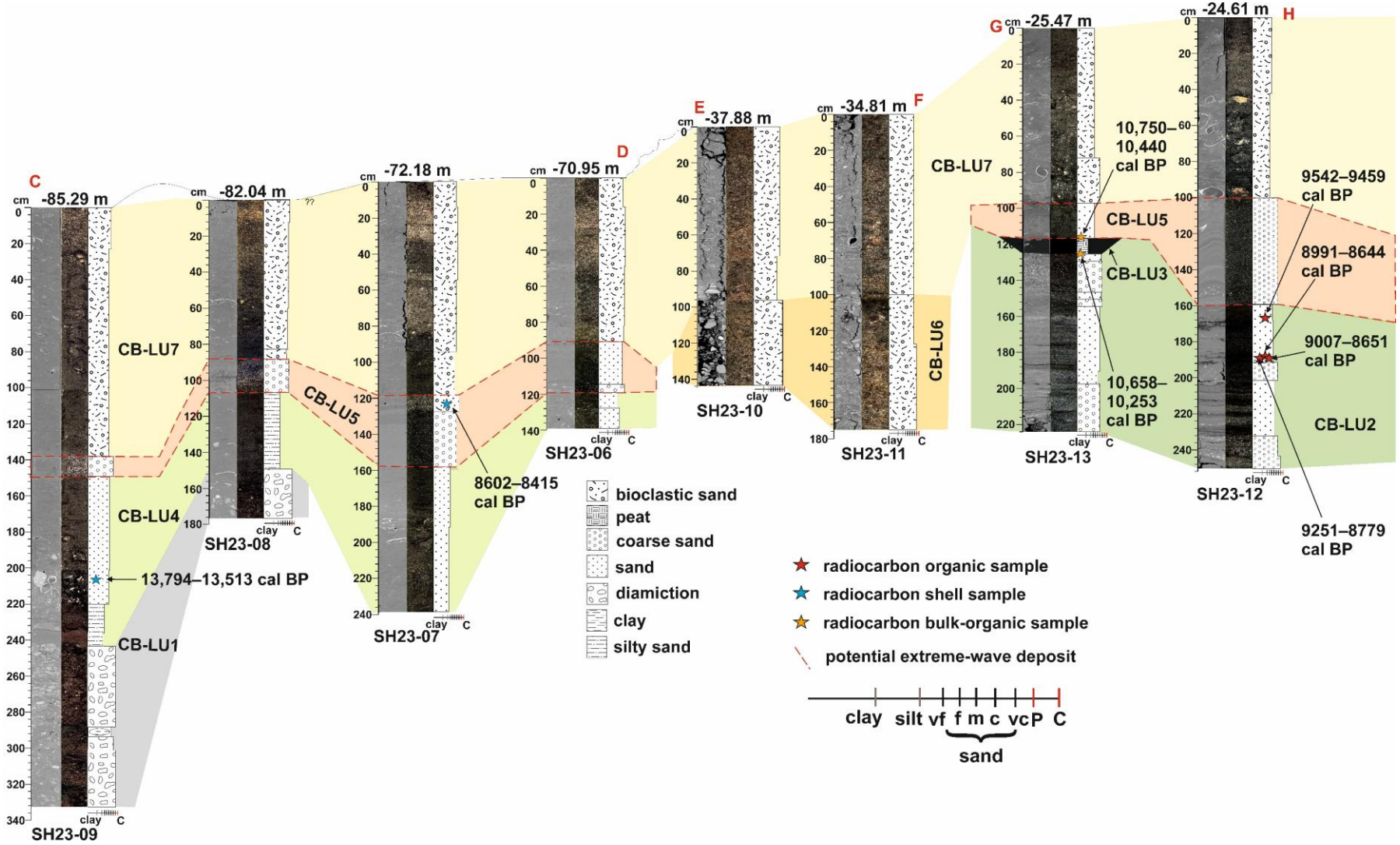

Figure 7. Core transect across Colgrave Sound/Basta Voe. Every core is shown with, from left to right, a high-resolution CT scan, a color-calibrated linescan image and a litholog, which is based on visual core description and interpretation. Shifts in vertical position of the cores along the transect highlight the differences in water depth at the core locations but are not to scale. Calibrated radiocarbon ages are indicated. Potential extreme-wave event deposits (?) are marked in orange with red dashed line.

4.3 Yell Sound

4.3.1 Morphology

The multibeam bathymetry of Yell Sound reveals a complex seafloor morphology, with water depths reaching 90 m b.s.l. in the northern sector where the system opens toward the ocean. Toward the south, depths decrease to <30 m b.s.l. near the sound entrance before increasing again farther into the sound. Overall, Yell Sound comprises a broad, north–south-oriented depression bounded by steep flanks and irregular bedrock-controlled ridges and highs, some of which protrude above sea level as small islands. These ridges subdivide the system into interconnected sub-basins. Water depths of over 100 m are attained in two north-south oriented elongated inner sub-basins (i.e. a western and an eastern sub-basin) that are separated by a central bedrock high. To the north, the shallower extensions of these sub-basins bend to NE-SW and NW-SE orientations and intersect, creating an X-shaped basin that opens toward the shelf break. The seafloor of the sub-basins is generally flat to locally mounded (Fig. 8).

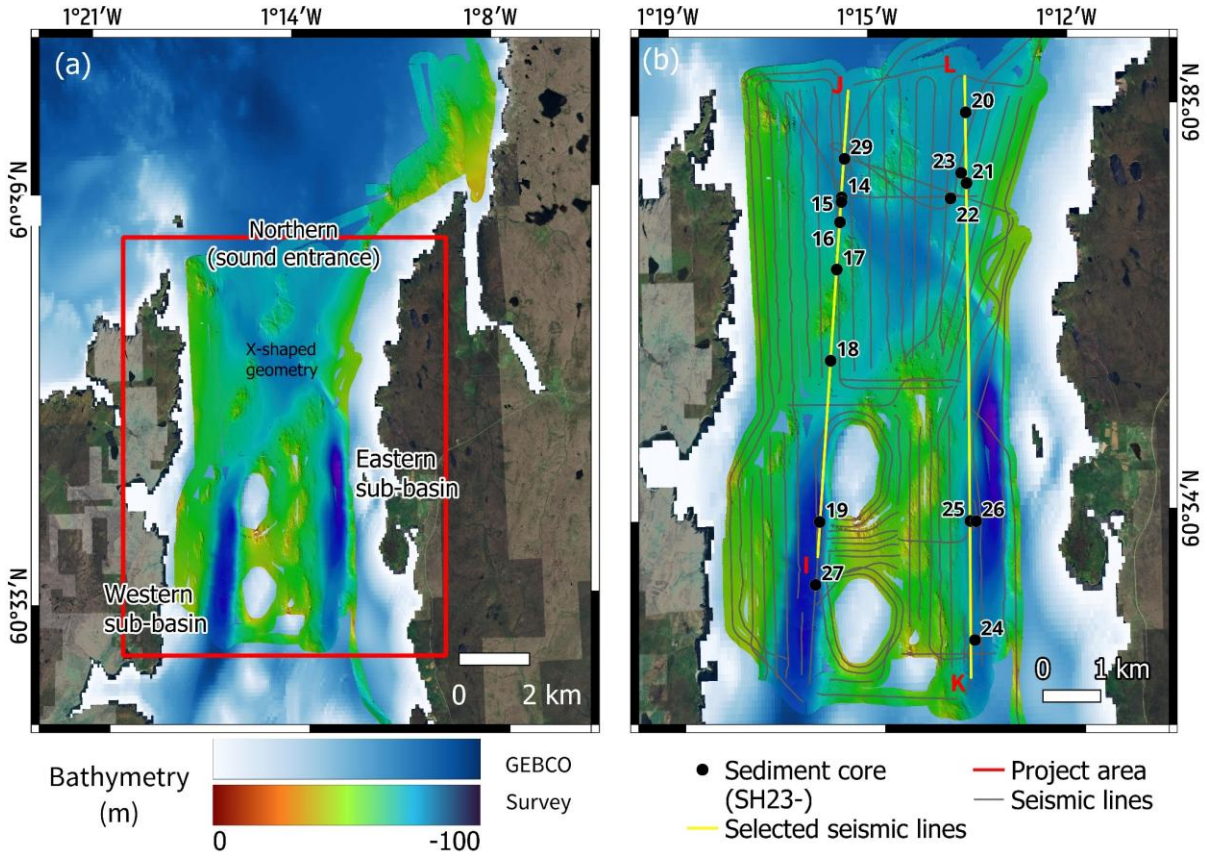

Figure 8. Bathymetric and seismic survey lines from Yell Sound. (a) Multibeam bathymetry overlain on 2025 grid with color gradients representing water depth (GEBCO Compilation Group, 2025), color-coded to illustrate water depth. (b) Seismic lines shown in Figs. 9, 10 (I–J, and K–L), along which sediment cores were collected to ground-truth stratigraphic interpretations, are highlighted in yellow.

4.3.2 Seismic stratigraphy

The 62 seismic profiles collected across Yell Sound cover around 311 km of survey lines (Fig. 8b). These data reveal the internal stratigraphic architecture of the basin, showing multiple depocenters separated and bounded by irregular bedrock highs. Seismic lines I–J (western sub-basin; Fig. 9) and K–L (eastern sub-basin; Figs. 8–10) illustrate the stratigraphic configuration and show six distinct seismic units (YS-SU1 to YS-SU6) that can be traced laterally across much of the sound:

- YS-SU1 forms the acoustic basement and is observed throughout Yell Sound. It is characterized by chaotic, low-amplitude internal reflections that gradually fade downward a few ms TWTT below the upper boundary. The top of the unit is an irregular, high-amplitude reflection exhibiting rugged relief with local highs and depressions. Many of the irregular highs correspond to bedrock exposed at the seafloor. YS-SU1a is a local sub-unit in the eastern part of Yell Sound. It forms a prominent mounded body overlying the bedrock surface and is onlapped by younger seismic units. It has a lateral extent of ca. 100 m and reaches a thickness of 10 ms TWTT. The sub-unit exhibits an irregular, transparent internal reflection pattern, which separates it from the surrounding sedimentary units, indicating that it represents a discrete stratigraphic body.
- YS-SU2 directly overlies the basement and infills all major overdeepened depressions. The unit occurs in the southern part of both the western and eastern sub-basins as well as in the northern sector, which is presently connected to the open ocean. Its seismic facies ranges from transparent to weakly stratified, with low- to medium-amplitude reflections that onlap against adjacent bedrock highs. YS-SU2 thickens markedly within the deepest depressions, reaching a thickness of 10 to locally 30 ms TWTT, while remaining thin or absent over structural highs. A gradual lateral change toward more continuous internal reflections is observed in the northern part of the basin. In the north of western sub-basin the unit shows a more chaotic facies with prograding clinoforms.
- YS-SU3 overlies YS-SU2 and occurs within several depressions in both the western and eastern part of Yell Sound. In the northern part of the western sub-basin, the unit is characterized by medium-amplitude, parallel to sub-parallel reflections that are laterally continuous across large areas. Further to the northwest, YS-SU3 locally has a mounded geometry. The upper part of the mound is truncated by the upper unconformity. In contrast, in the southern part of the western sub-basin, YS-SU3 displays lower to medium reflection amplitudes and a more irregular, locally discontinuous internal reflection character. Locally, YS-SU3 thickens along basin margins and drapes over irregular topography. Immediately above its base, a relatively thin (<0.5 ms TWTT) acoustically stratified sub-unit occurs in some areas (e.g. near SH23-16) characterized by medium-amplitude reflections. Overall, YS-SU3 reaches a maximum thickness of up to 25 ms TWTT in the northern part of the western sub-basin, whereas in its southern part it is considerably thinner, with a maximum thickness of ca. 5 ms TWTT.
- YS-SU4 overlies YS-SU3 and, locally, YS-SU2 in the inner part of the sound, and it is present in both the western and eastern sub-basins. The base of YS-SU4 is marked by an irregular unconformity, which is particularly well developed in the western sub-basin. Here, the lower boundary truncates underlying reflections and locally displays erosional relief, especially where YS-SU4 builds into mounded geometries. Internally, the unit is characterized by high-amplitude reflections with variable continuity and locally disrupted internal patterns. YS-SU4 is laterally extensive across the basin and typically attains a thickness of 3 ms TWTT, but it thickens to up to 10 ms TWTT within a NE–SW-oriented depocenter where the sub-basins intersect in the northern part of the sound. The unit is traceable across multiple depocenters.
- YS-SU5 occurs directly above YS-SU4 in the northern part of the western sub-basin. It is characterized by a nearly transparent facies or by a weakly stratified facies with low- to medium-amplitude reflections. It has a sharp basal contact separating it from the more chaotic, higher-amplitude reflections below. Seismic unit YS-SU5 is generally <2 ms TWTT thick.
- YS-SU6 forms the uppermost seismic unit across Yell Sound. It is characterized by laterally continuous, medium- to high-amplitude, parallel reflections. While the unit is relatively thin over structural highs, its thickness varies substantially across the basin. In several areas, including the northern sector and along the north-western margin, YS-SU6 thickens markedly, locally reaching 10–15 ms TWTT (Fig. 9). In addition, the unit displays pronounced mounded geometries, particularly within the southern part of eastern sub-basin (Fig. 10). Locally, erosional lower boundaries are observed, especially in the middle part of western sub-basin, where YS-SU6 overlies older units (Fig. 9c).

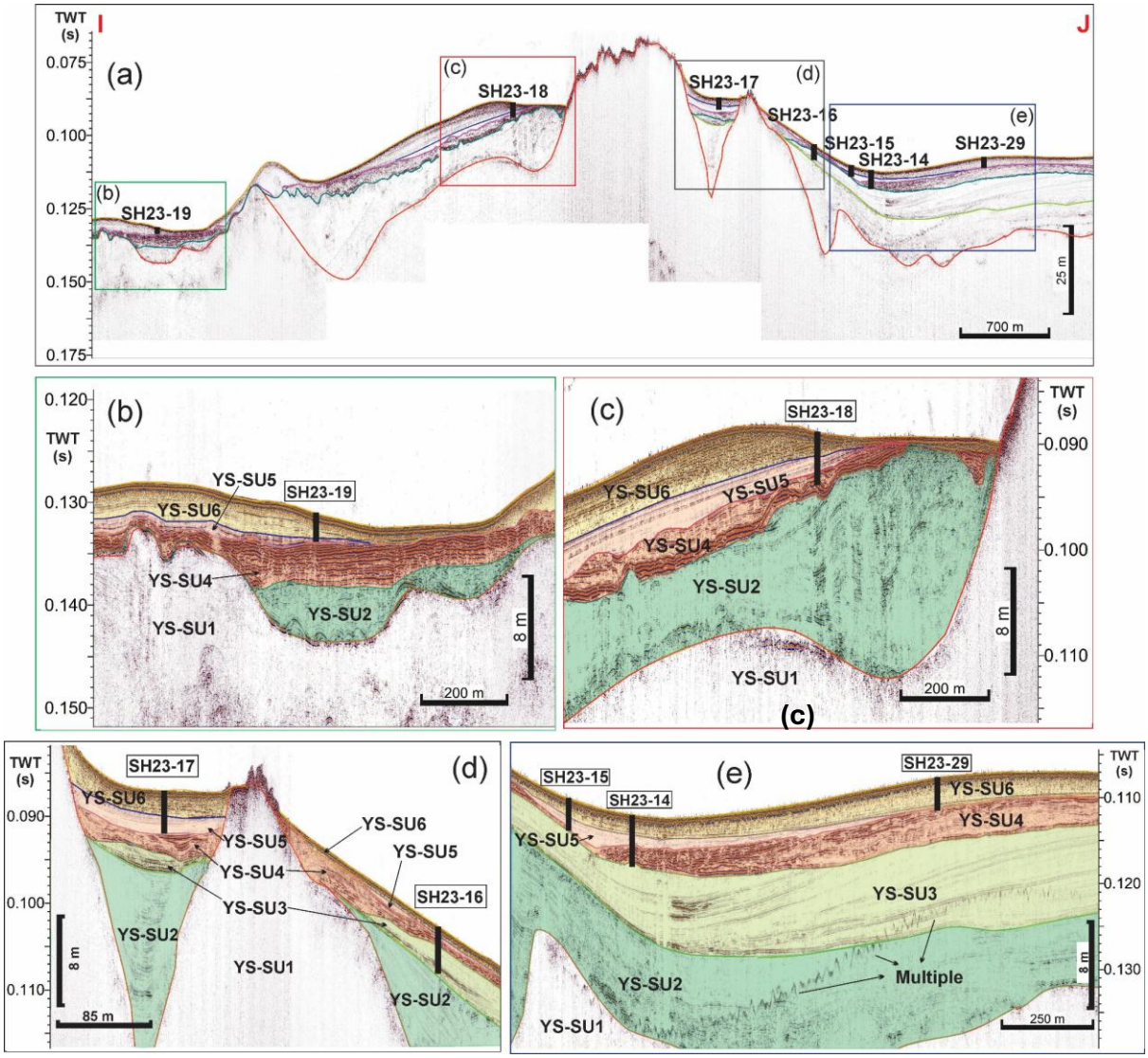

Figure 9. Sub-bottom profile from the western inner sub-basin of Yell Sound. (a) Uninterpreted seismic profile along survey line H–I, showing the overall basin geometry and sediment stratigraphy. The locations of coring sites SH23-14 to SH23-19 and SH23-29 are indicated. Panels (b), (c), (d) and (e) show interpreted versions of sections of the same profile, illustrating the six seismic units YS-SU1 to YS-SU6.

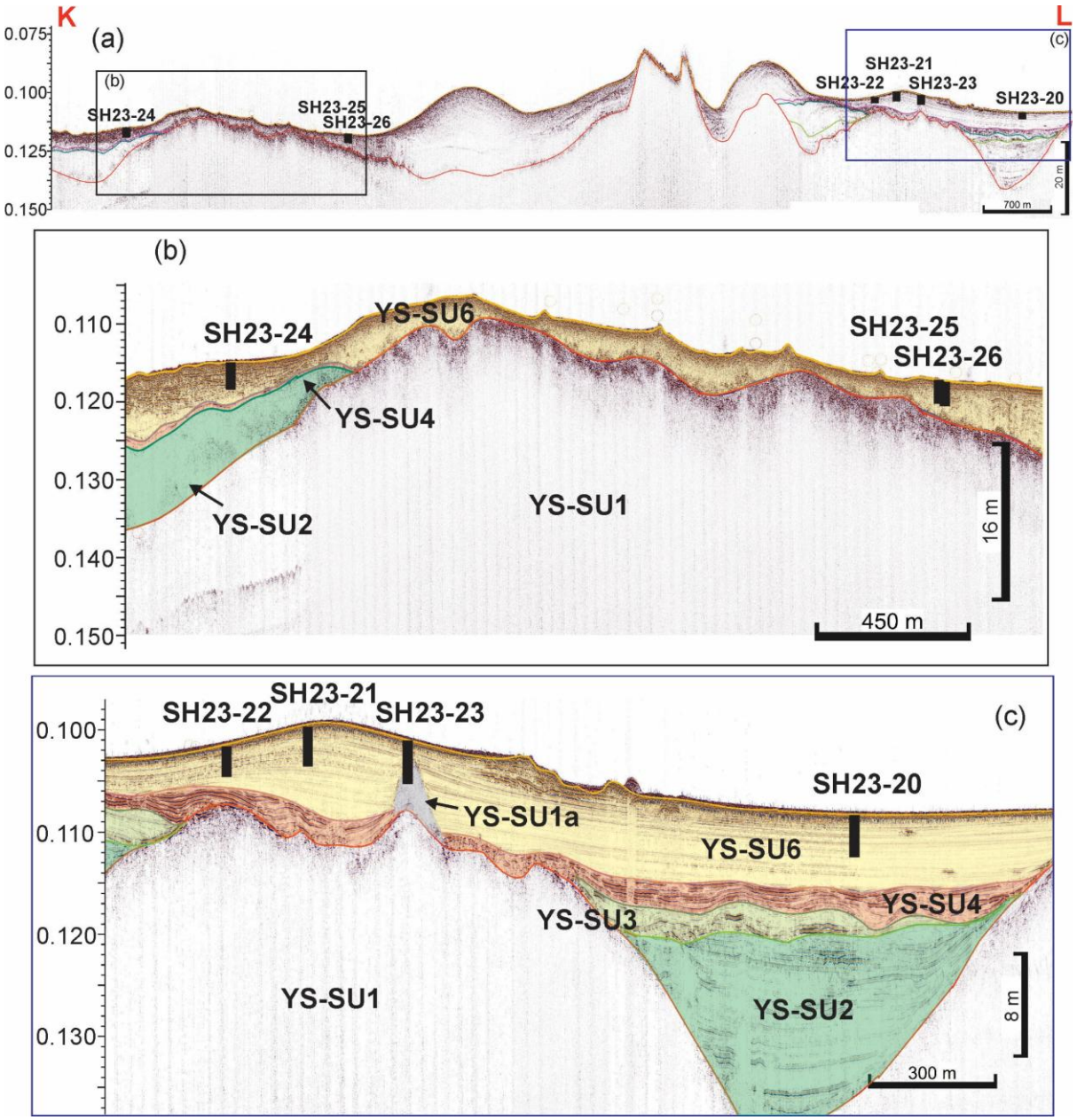

Figure 10. Sub-bottom profile from the eastern inner sub-basin of Yell Sound. (a) Uninterpreted seismic profile along survey line J–K, showing the overall basin geometry and sediment stratigraphy. The locations of coring sites SH23-24, SH23-25 and SH23-26 are indicated. Panels (b) and (c) show interpreted versions of sections of the same profile, illustrating the seismic units YS-SU1, YS-SU1a, YS-SU2, YS-SU3, YS-SU4, and YS-SU6.

4.3.3 Lithological units and core-to-seismic correlation

Of the 15 coring sites in Yell Sound (Fig. 8b), eight (SH23-14, SH23-15, SH23-16, SH23-17, SH23-18, SH23-19, SH23-27 and SH23-29) are located in the western part of the sound, and seven (SH23-20, SH23-21, SH23-22, SH23-23, SH23-24, SH23-25 and SH23-26) in the eastern part. Cores from the western part of the sound provide the clearest stratigraphic tie to the seismic units, as they penetrate a greater thickness of the sedimentary sequence and intersect multiple lithological and seismic units (Fig. 9). In contrast, core penetration in the eastern sub-basin is generally limited, and the recovered sequences predominantly capture only the uppermost units due to the considerable thickness of these deposits, with the exception of SH23-23.

Eight lithological units (YS-LU1 to YS-LU8) were identified in the coring transect in the western part of Yell Sound (Fig. 11) and correlated with the seismic units recognized on the sub-bottom profiles (Fig. 9). An additional lithological unit (YS-LU0) was identified only at one coring site in the eastern part of the sound (Fig. 10). These lithological units are described below in ascending stratigraphic order:

- YS-LU0 (not included on Fig. 11) occurs exclusively in the entrance of the eastern part of the sound and is only identified at site SH23-23, where it extends from 59.5 cm depth to the base of the core. It consists of well-sorted medium grey silt with faint mm-scale laminations and good sorting. Shell fragments are rare but become slightly more common toward the base. This unit corresponds to seismic sub-unit YS-SU1a.
- YS-LU1 was retrieved only at site SH23-16. It consists of bioclastic gravel and coarse sand with broken mollusk shells embedded in a fine sand matrix. The unit is massive and has a gradational upper boundary. It corresponds to the high-amplitude reflection at the base of YS-SU3.
- YS-LU2 overlies YS-LU1 at site SH23-16 and is also present at site SH23-14. It comprises dark grey silty sand to sandy silt. The unit is massive, contains limited bioclastic material, and shows distinct contacts with underlying and overlying units. It reaches a thickness of 80 cm at site SH23-16. An articulated bivalve was recovered from this unit at 133–136 cm depth at site SH23-16. This unit corresponds to seismic unit YS-SU3.
- YS-LU3 is a distinctive sand-dominated unit present at sites SH23-14, SH23-15, SH23-16 and SH23-18. Where fully preserved, the unit consists of coarse, poorly sorted gravelly sand with a sharp basal boundary, overlain by a fine- to medium-grained laminated sandy interval, and capped by poorly sorted bioclastic sand with a bright whitish color. The thickness and internal composition of the unit vary considerably between cores. This lithological unit corresponds to seismic unit YS-SU4.
- YS-LU4 occurs at sites SH23-14, SH23-15, SH23-16, SH23-17, SH23-18, SH23-19 and SH23-29. It consists of dark minerals with slightly finer grained sand compared to underlying and overlying units. The unit is well sorted and scattered with less shell fragments. Thickness varies considerably, and reaches a maximum around 90 cm at site SH23-17. This unit corresponds to seismic unit YS-SU5.
- YS-LU5 forms the uppermost unit at sites SH23-14, SH23-15, SH23-16, SH23-17, SH23-18, SH23-19 and SH23-29, and is also present in the eastern part of the sound (SH23-21 to SH23-26). It consists of light grey to yellowish bioclastic sand, is medium- to coarse-grained, generally poorly sorted, and dominated by fragmented mollusks. The unit has a gradual basal contact and varies in thickness across the sound between 40 cm to ca. 200 cm. At most sites, this unit corresponds to seismic unit YS-SU6.

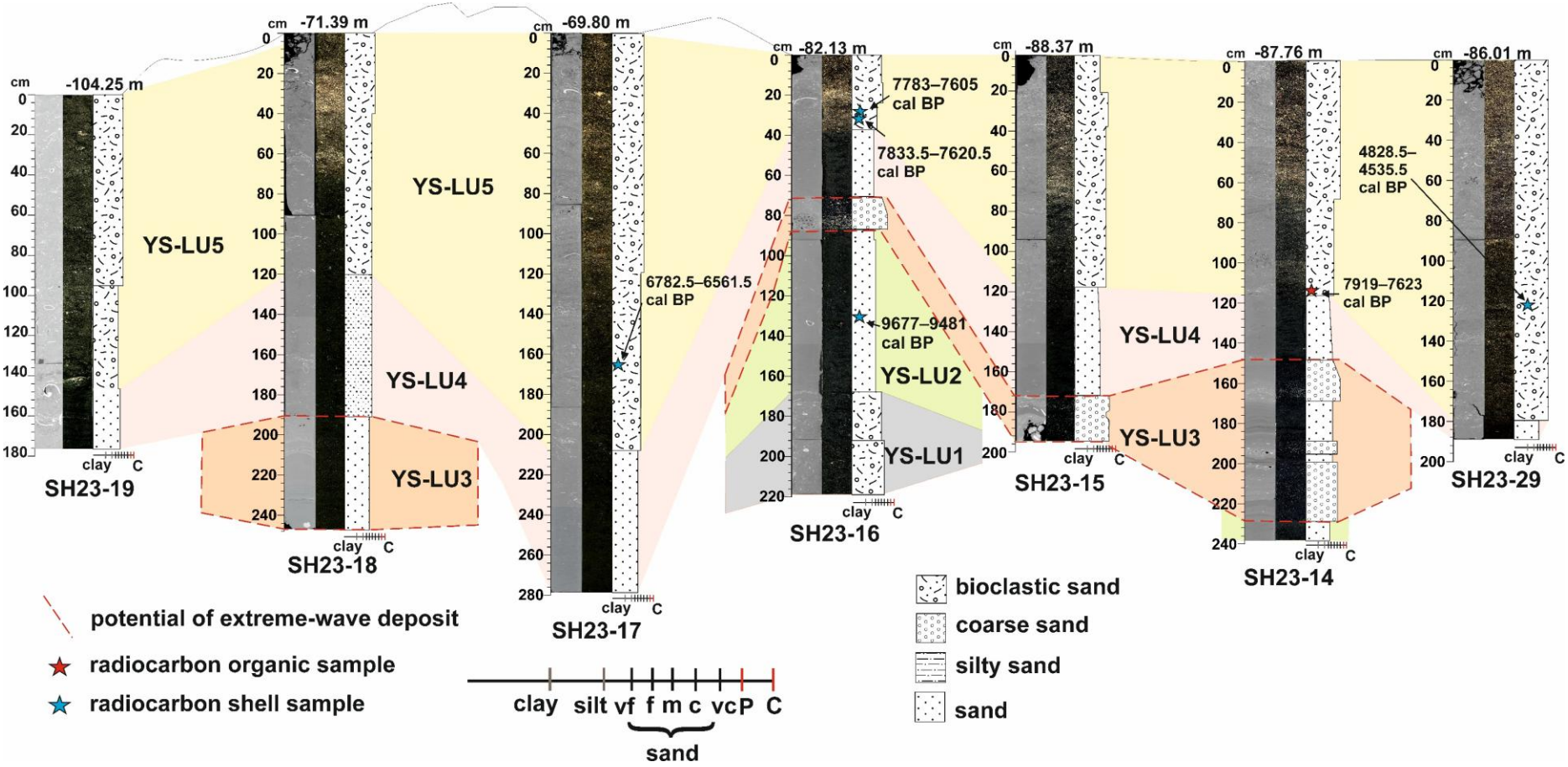

Figure 11. Core transect across the western sub-basin of Yell Sound. It provides the best representation of lithological variability and enables robust core-to-core correlation due to differences in sediment penetration and stratigraphic completeness among the cores. Each core is shown with, from left to right, a high-resolution CT scan, a color-calibrated linescan image, and a litholog derived from visual core description and interpretation. Shifts in vertical position of the cores along the transect highlight the differences in water depth at the core locations but are not to scale. Calibrated radiocarbon ages are indicated. Potential extreme-wave event deposits are marked in orange with red dashed line.

5 Discussion

5.1 Interpretation

5.1.1 Dury Voe: stratigraphy and evolution of the depositional environment

Multibeam bathymetry and sub-bottom profiler data show that sediment accumulation in Dury Voe is patchy. Sediments are preferentially confined to a series of discrete sub-basins bounded by topographic highs associated with exposed bedrock. This configuration reflects strong spatial variability in accommodation space and sediment distribution controlled by the irregular bedrock morphology, a characteristic feature of formerly glaciated basins (Bradwell et al., 2019; Burschil et al., 2019; Syvitski et al., 1987).

At the base of the sedimentary sequence, seismic sub-unit DV-SU1a is interpreted as the acoustic signature of a coarse-grained deposit overlying the metamorphic bedrock (DV-SU1) in the basin. The irregular high-amplitude upper reflection, the chaotic, low-amplitude internal reflections and the very limited acoustic penetration suggest a strongly consolidated deposit with a rugged upper surface. Seismic sub-unit DV-SU1a is cored at sites SH23-02 and SH23-30, where the basal lithological unit consists of sub-rounded quartz and lithic pebbles, derived from metamorphic and metasedimentary rocks, in a matrix of muddy sand (i.e., DV-LU1). This massive unit lacks internal structure and exhibits a sharp upper contact, which are characteristics typical for glacial or glaciofluvial deposits (Bradwell and Stoker, 2015; Hogan et al., 2020). At site SH23-30, in the deeper waters of the outer fjord, DV-LU1 is overlain by DV-LU2, of which the coarse sand with smaller pebbles and might indicate reworking of glacial or glaciofluvial material during an early phase of the marine transgression (Hogan et al., 2020).

In the western sub-basin of the voe, DV-SU1 (or DV-SU1a) is overlain by seismic unit DV-SU2, which represents the initial phase of sediment accumulation within localized depressions in the basement topography. At sites SH23-05 and SH23-02, this unit consists of silty clay with uniform texture and color (i.e., DV-LU3), indicating prolonged low-energy sedimentation. The ponded seismic geometry and stratified facies with low- to medium-amplitude reflections of DV-SU2 further support deposition within a confined and low-energy basin setting. The absence of grading or internal structures, together with its occurrence as the basal infill of an isolated depression in a confined inner-fjord setting, suggests a possible lacustrine origin (Syvitski et al., 1987; Syvitski and Shaw, 1995), although this interpretation still requires confirmation through microfossil or geochemical analyses. If the depression was already connected to the sea at the time of deposition, the environment may instead have been estuarine or a sheltered intertidal embayment that later evolved into a shallow marine setting. At site SH23-02, the base of DV-SU2 (i.e., DV-LU3) is dated to 10333–10176 cal BP. The prominent high-amplitude reflection marking the sharp transition from DV-SU2 to DV-SU3 is interpreted as marking the marine transgression in this sector of the voe. This transition occurs at 39.1 m b.s.l.

Seismic unit DV-SU3 forms a prominent unit across the study area. It occurs as the upper infill of localized depressions in the basement topography but it is also present outside these depressions. The unit consists of acoustically well-stratified deposits and is composed of bioclastic marine sand enriched in shell hash and coarse fragments (i.e., DV-LU4). This represents a clear change in grain size and composition relative to the underlying silty clay of DV-LU3 and indicates a shift toward higher-energy depositional conditions. The mounded geometry and laterally variable thickness of DV-SU3 suggest deposition in a shallow marine environment influenced by persistent bottom currents.

The two high-amplitude intervals (HAI1 and HAI2) within DV-SU3 consist of poorly sorted sand that is coarser than the surrounding sediments of DV-SU3, contain larger angular shell fragments, display sharp lithological contrasts with the surrounding sand, and show normal grading. These characteristics suggest deposition during high-energy events such as storm surges or tsunamis. Similar sedimentary

signatures have been described in nearby onshore environments (Bondevik, et al., 2005; Engel et al., 2024).

The sand that makes up DV-SU3, just underneath the oldest of these coarse-grained event deposits at site SH23-02, is dated at 8311–8017 cal BP, suggesting that the overlying high-energy event deposit could represent the Storegga Slide tsunami (ca. 8150 cal BP; Bondevik et al., 2012). This is in line with the observations by Earland et al. (2024), who identified a similar coarser-grained layer in the deeper waters of the nearby Fetlar Basin of Shetland and dated it as the Storegga tsunami deposit.

The upper coarse-grained event deposit is slightly darker in tone, visually more compact, and contains fewer shell fragments, suggesting somewhat different depositional conditions. This layer has not been dated directly, but the upper part of DV-LU3, located about 25 cm above the event layer at site SH23-05, yields an age of 1346–1178 cal BP. It is therefore not unreasonable to attribute this second event deposit to the ca. 1500 cal BP tsunami documented onshore in Dury Voe (Bondevik et al., 2005; Dawson et al., 2006).

Seismic unit DV-SU4 corresponds to the most recent sediments below the modern sediment-water interface. The high-amplitude, rough-textured and laterally continuous reflections that characterize this unit suggest active processes, including ongoing sedimentation and possible reworking by waves or bottom currents. The sediments consist of unconsolidated organic-rich fine sand. Bulk samples dated at site SH23-05 yield an age of 1532–1403 cal BP at 17.5 cm below the surface. This age may be slightly too old due to sediment reworking, as fossil evidence from infaunal bivalves: *Thyasira flexuosa* (López-Jamar et al., 1987) recovered from the uppermost sediment layer at 17.5 cm depth, yielded a modern radiocarbon age. The upper unit is therefore interpreted to represent modern sedimentation under relatively stable environmental conditions.

5.1.2 Colgrave Sound/Basta Voe: stratigraphy and evolution of the depositional environment

The multibeam bathymetry and sub-bottom profiles show that, like in Dury Voe, sediment distribution in Colgrave Sound/Basta Voe is highly patchy, with thicker sediment successions confined to sub-basins bounded by bedrock highs.

At the base of the sedimentary sequence, seismic sub-unit CB-SU1a corresponds to a compact, massive pebbly sand to gravel with sub-rounded quartz and lithic clasts (lithological unit CB-LU1 at sites SH23-09 and SH23-08). The presence of a high-amplitude reflection overlying internally chaotic, low-amplitude reflections that fade downward provides seismic evidence for a consolidated substrate. Together with the rugged relief of the upper surface, this supports the interpretation of a consolidated glacial till resting directly on bedrock (CB-SU1), consistent with ice-proximal or subglacial deposition (Bradwell and Stoker, 2015).

Overlying this, seismic unit CB-SU2 records the initial postglacial infill of basement depressions. In the southern deep basin (e.g. sites SH23-06, SH23-07, SH23-08, SH23-09) it is represented by a massive sandy silt with marine shell fragments (i.e., CB-LU4). An articulated bivalve shell (*Mya truncata*), commonly occurring in intertidal environments and down to a water depth of ca. 10 m (Oliver et al., 2016), was recovered from site SH23-09 at a depth of 87.3 m b.s.l. It yields an age of 13794–13513 cal BP, providing evidence for estuarine, lagoonal to marginal marine conditions at the time of deposition. In the northern shallow sector (e.g. sites SH23-12, SH23-13) the correlative lower infill consists of fine to medium micaceous sand with stratified/wavy lenticular bedding (i.e., CB-LU2), indicating strong terrestrial input. Combined with the absence of marine shell fragments we interpret this unit to be deposited in a deltaic-fluvial environment (Nichols, 2009). At site SH23-13, CB-LU2 is overlain by a peat horizon (i.e., CB-LU3, at a depth of ca. 26.7 m b.s.l.), with ages of 10658–10253 cal BP (base of the peat) and 10750–10440 cal BP (top of peat), indicating early-transgressive nearshore marsh/peatland development prior to full marine inundation (Shennan and Horton, 2002; Smith et al., 2019). In contrast to the more terrestrially influenced northern sector deposits, CB-LU4 reflects an earlier establishment of marine influence in the deeper southern basin areas of Colgrave Sound–Basta Voe.

A pronounced shift follows with seismic unit CB-SU3 (i.e., CB-LU5). This unit shows a sharp basal contact, poor sorting, locally abundant angular shell fragments and normal grading. Importantly, CB-SU3 forms a laterally continuous, high-amplitude seismic unit traceable across both Colgrave Sound and Basta Voe, in a wide range of water depths. These sedimentological and seismic characteristics indicate rapid deposition under high-energy conditions consistent with an extreme-wave event, such as a tsunami or major storm surge, involving erosion, sediment entrainment, and subsequent settling of reworked material during flow deceleration and backwash (Dawson & Stewart, 2007; Morton et al., 2007). In Colgrave Sound, at site SH23-07, shells within CB-LU5 yield an age of 8602–8415 cal BP, which is a consistent *terminus ante quem* for the Storegga tsunami (Bondevik et al., 2012). In Basta Voe, at site SH23-12, sands immediately beneath the event layer return older ages of 9542–9459 cal BP, while several shell ages within the unit indicate incorporation of reworked material during emplacement (e.g., 9251–8779 cal BP, 9007–8651 cal BP and 8991–8644 cal BP). Together, these ages provide a maximum-age constraint consistent with a potential Storegga-related event deposit for unit CB-LU5.

Seismic unit CB-SU4 forms the uppermost part of the sedimentary sequence and corresponds to lithological units CB-LU6 and CB-LU7. CB-SU4 displays well-developed mounded and asymmetric geometries, particularly in the deeper parts of the basin, which suggest they were shaped by persistent bottom currents and allow them to be interpreted as sediment drifts (Knutz and Cartwright, 2003). In Colgrave Sound, the unit consists mainly of medium- to coarse-grained bioclastic sand dominated by bryozoans and bivalve shell debris, consistent with deposition under high-energy marine conditions influenced by bottom currents (Farrow et al., 1984). In contrast, in the shallower Basta Voe, CB-SU4 contains coarser bioclastic sand with abundant large bivalve fragments up to 12 cm in diameter, reflecting reworking under higher-energy shallow-marine conditions. Despite the 60 m difference in water depth and hydrodynamic energy between the two sites, the strong, laterally continuous reflections of CB-SU4 demonstrate that both facies represent the same upper marine drift unit deposited during the establishment of fully marine conditions after the Storegga event.

5.1.3 Yell Sound: stratigraphy and evolution of the depositional environment

The elongated depressions in both the western and eastern sub-basins of Yell Sound, together with a distinctive X-shaped basin geometry in the northern sector where the sound opens toward the open ocean (Fig. 9), reflect strong inherited structural control within the tectonically complex Caledonian framework of Shetland, where the major NE–SW- and N–S-trending fault systems have influenced bedrock morphology (Mykura et al., 1976). Prominent bedrock highs separating the sub-basins, particularly in the northwestern and eastern parts of the sound, are consistent with this structural inheritance.

However, comparison of basement depth, total sediment thickness (Supp. Fig. S1), and seismic stratigraphy demonstrates that sediment distribution does not simply mirror basement relief. Although some structurally deep areas contain thick sediment successions, other deep depressions remain sediment-starved, while substantial sediment accumulations also occur above intermediate basement depths. In both sub-basins, elongated sediment bodies and N–S-oriented drift mounds are developed along the basin axes, whereas adjacent bedrock highs remain sediment-poor (Figs. 9, 10). Seismic profiles show that the upper units are characterized by high-amplitude, laterally continuous reflections and mounded geometries, indicating enhanced sediment redistribution by bottom currents following the marine transgression. The X-shaped northern basin geometry and associated sediment patterns likely reflect the combined influence of inherited structural relief and hydrodynamic processes.

At the base of the succession, seismic unit YS-SU1 is interpreted as metamorphic basement rocks of the Dalradian Supergroup (Mykura et al., 1976). The rugged basement morphology and pronounced local highs and depressions likely result from selective glacial erosion and overdeepening during the

last glaciation, guided by pre-existing fault zones and lithological contrasts within the Caledonian structural framework (Hall et al., 2013; Stein, 1988). Locally, at the entrance of the eastern part of the sound, sub-unit YS-SU1a, with its distinct mounded geometry, has been preserved on top of a local bedrock high. This remarkable feature likely represent a glacially reworked (pushed) pro- or peri-glacial deposit (i.e., YS-LU0).

Overlying the acoustic basement (YS-SU1), YS-SU2 forms the lowermost sedimentary infill. The unit thickens into major overdeepened depressions in both the western and eastern sub-basins and thins or pinches out over intervening basement highs. Its seismic facies is acoustically stratified with low- to medium-amplitude reflections that onlap against bedrock topography. YS-SU2 was not recovered due to the limited penetration depth of the vibrocorer. Taken together, the ponded geometry, stratified seismic character, and stratigraphic position below more clearly current-dominated marine units suggest that YS-SU2 represents an early phase of restricted to marginal marine basin infill, deposited during deglaciation and initial marine flooding of the basin. Comparable acoustically stratified sediments infilling glacially eroded bedrock basins have been documented in e.g. West Greenland fjords (Ó Cofaigh et al., 2016) and in Newfoundland (Forbes et al., 1993).

The sandy deposits of YS-LU2, recovered at sites SH23-14 and SH23-16, together with the laterally continuous, medium-amplitude, parallel to sub-parallel seismic reflections of seismic unit YS-SU3, mark the basin-wide establishment of marine conditions during the early Holocene transgression. Locally developed mounded geometries within YS-SU3 suggest an increasing influence of bottom currents, consistent with progressively more open-marine conditions. Radiocarbon ages recovered from YS-LU2, at site SH23-16, at a depth of 83.4 m b.s.l., indicate that this site was already in an open-marine environment before 9677-9481 cal BP.

In several locations, seismic unit YS-SU4 forms a distinct, high-amplitude package overlying YS-SU3 and, locally, YS-SU2 and corresponds to coarse, poorly sorted sand with abundant angular shell fragments and a chaotic internal structure (i.e., YS-LU3). YS-SU4 is separated from the underlying units by a regionally expressed erosional unconformity, particularly well-developed in the western sub-basin (Fig. 9c), where truncation of underlying reflections and pronounced relief at the basal contact are evident. The combination of a sharp erosional basal contact, chaotic internal fabric, and a composition rich in shell fragments indicates deposition under turbulent, high-energy conditions, consistent with rapid sediment emplacement and erosion (Costa et al., 2021b; Feist et al., 2023). Together with its basin-wide extent and stratigraphic position within the marine succession, these characteristics suggest that YS-SU4 records an abrupt depositional event, most plausibly related to an extreme-wave process such as a tsunami or a major storm surge (Bondevik et al., 2005; Earland et al., 2024; Sharrocks et al., 2025).

Seismic unit YS-SU5 forms a thin, acoustically almost transparent package above YS-SU4.At coring sites SH23-14 to SH23-17 and SH23-29 it consists predominantly of medium sand with moderate sorting and normal grading (i.e., YS-LU6), reflecting a systematic decrease in depositional energy following the main high-energy pulse recorded by YS-SU4. This sedimentary character is consistent with deposition during the waning-flow phase of the same extreme event (Costa et al., 2021b; Feist et al., 2023). Radiocarbon ages obtained from material immediately overlying this unit yield ages of 7919–7623 cal BP at site SH23-14 and 7783–7605 cal BP at site SH23-16. These ages are consistent with interpretation of both units (YS-SU4 and YS-SU5) being related to the Storegga Slide tsunami (Bondevik et al., 2005; Dawson et al., 2020; Earland et al., 2024)

Seismic unit YS-SU6 is characterized by high-amplitude, laterally continuous reflections and locally developed moat-and-mound geometries, indicative of deposition under shallow-marine conditions

influenced by bottom currents. The unit consists primarily of bioclastic medium sand rich in fragmented marine shells (i.e., YS-LU5), but shows pronounced lateral variability in sedimentary facies. Radiocarbon ages obtained from this unit, including 6782–6561 cal BP at site SH23-17 and 4828–4535 cal BP at site SH23-29, indicate progressive sediment accumulation during the mid- to late Holocene (Fig. 11). The sharp upper boundary, marked by a high-amplitude reflection corresponding to the modern seafloor, together with the presence of sediment mounds, reflects a well-established shallow-marine system dominated by sustained bottom-current reworking during the final stage of sedimentation in Yell Sound.

5.2 Post-glacial evolution of the depositional environment

5.2.1 Basin-wide stratigraphic consistency and regional framework

Across the three investigated areas (Dury Voe, Colgrave Sound/Basta Voe, and Yell Sound), a broadly comparable post-glacial stratigraphic succession is recognized, despite differences in basin geometry, water depth, and hydrodynamic setting. In all areas, sedimentation is strongly controlled by inherited bedrock morphology, with sediment preferentially accumulating within overdeepened depressions bounded by bedrock highs that remain largely sediment-starved. This pattern is characteristic of formerly glaciated valleys and embayments, where structural inheritance and glacial overdeepening exert a first-order control on post-glacial sediment distribution (Bradwell et al., 2019; Syvitski et al., 1987; Trottier et al., 2020). Comparable relationships between basement relief and sediment infill have been documented in e.g. fjords of western Norway, Svalbard, and Alaska (Husum et al., 2019). While this depositional framework is well established for deeper fjord environments, it has rarely been documented in detail within shallow nearshore and voe systems such as those in Shetland, where sediment distribution is additionally strongly influenced by limited basin accommodation space.

Within this framework, the sedimentary succession in each basin can be subdivided into four main stages: (i) a pre-marine substrate developed on crystalline bedrock, locally mantled by glacial or glaciofluvial deposits; (ii) an initial post-glacial infill deposited under low-energy conditions within isolated or semi-restricted basins; (iii) a transitional phase marked by the marine transgression and increasing hydrodynamic influence; and (iv) an upper succession dominated by marine sands that form laterally extensive, current-influenced mounded drift geometries.

5.2.2 Nature of the pre-marine substrate and early transgressive infill

The acoustic basement in all three study areas likely corresponds to the metamorphic rocks of the Dalradian Supergroup. In several locations, this basement is overlain by consolidated coarse-grained deposits interpreted as glacial or glaciofluvial in origin. They are best developed in Dury Voe (DV-LU1) and locally in Colgrave Sound (CB-LU1), whereas they are not recovered in parts of Yell Sound (YS-SU1) since the cores did not reach this facies.

Above this substrate, the earliest post-glacial sediments record reduced-energy depositional conditions, reflecting limited basin connectivity during the initial stages of deglaciation (Figs. 12a, b). Comparable low-energy basal infill has been documented from glaciated fjord and nearshore settings such as western Norwegian fjords (e.g. Hardangerfjord and Sognefjord), Svalbard fjords (e.g. Isfjorden), and Alaskan fjords (e.g. Glacier Bay), where fine-grained sediments accumulated within isolated or semi-restricted basins prior to marine transgression (Balascio et al., 2011; Poiré et al., 2018). In Dury Voe, this phase is represented by silty clay infilling isolated depressions (DV-SU2/DV-LU3; Fig. 3), consistent with sedimentation in a lacustrine, estuarine, or sheltered embayment setting (Fig. 12c). The available proxies do not allow a clear distinction to be made between lacustrine, estuarine, or restricted marine environments during this phase. In Colgrave Sound and Basta Voe, equivalent

deposits exhibit greater lateral variability, ranging from lagoonal or estuarine sandy silts containing marine shells in deeper basins (CB-LU4) to fluvial–deltaic sands and peat development in shallow marginal areas (CB-LU2, CB-LU3; Fig. 7). In Yell Sound, early infill units comprising shell-bearing sediments (YS-SU2/YS-LU1–2; Figs. 10, 11) record a clear transition from restricted to increasingly marine conditions, consistent with progressive basin flooding during the onset of the marine transgression.

5.2.3 Marine transgression and onset of current-dominated sedimentation

Following the marine transgression during the early Holocene, all three basins record a shift from fine-grained, low-energy to sand-dominated, higher-energy sedimentation (Fig. 12d). This transition is expressed by laterally extensive seismic units characterized by parallel to sub-parallel reflections, increased reflection amplitudes, and the development of mounded or draped geometries. Such seismic characteristics reflect enhanced bottom-current activity associated with rising sea level, widening basin connectivity, and the establishment of persistent tidal and residual circulation patterns that promote sediment reworking and lateral transport rather than pure vertical aggradation (Bradwell and Stoker, 2015; Rebesco et al., 2014).

In several locations, sediment accumulation is spatially associated with current-scoured moats, developed along basin margins and around bathymetric highs, where bottom-current velocities are locally enhanced. These moats act as sediment bypass zones, flanking adjacent mounded sand accumulations (drifts) that form under reduced flow velocities on the down-current side of the circulation cell (Wilckens et al., 2023). In Dury Voe, this phase is represented by DV-SU3, which forms asymmetric mounds composed of marine sands and is interpreted as current-controlled sediment accumulation within a confined basin setting. In Colgrave Sound/Basta Voe, the equivalent unit (CB-SU4) develops into large, asymmetric sediment drifts, with systematic facies variations reflecting depth-dependent hydrodynamic energy and proximity to the open marine domain. In Yell Sound, equivalent units (YS-SU6) display pronounced lateral thickness variability and well-developed mounded geometries, particularly within the northern sub-basin, where basin geometry enhances current acceleration and sediment focusing. This effect is related to the confinement of bottom currents within elongate depressions in the voe and their deflection along basin margins, leading to locally increased flow velocities and preferential sediment accumulation on the down-current flanks of sediment drifts.

5.2.4 Spatial distribution of marine deposits: pockets and drifts

The spatial distribution of post-transgressive sediments highlights an evolution from early sediment infill confined to structurally controlled pockets to laterally extensive marine drifts (Fig. 12g). This pattern is consistently observed across all three study areas. Isohypses of the pre-marine surface and isopach maps of the marine units (Supp. Fig. S1) demonstrate that early accommodation space was controlled almost exclusively by inherited basement relief, with sediment preferentially accumulating within overdeepened depressions. In contrast, thickness patterns of the overlying marine units reflect increasing redistribution by bottom currents, resulting in sediment focusing that is partly decoupled from basement depth. This transition from structure-dominated to current-dominated processes has been corroborated in other glaciated fjord and nearshore systems following the early Holocene transgression (Bianchi et al., 2020; Bradwell and Stoker, 2016). In Yell Sound, comparison of basement depth and sediment thickness maps indicates that post-transgressive sediment accumulation is not strictly tied to basement relief, but is locally enhanced by current-driven focusing and erosion. Similar drift development above intermediate basement levels in Colgrave Sound suggests that bottom-current processes exert a secondary control on sediment distribution superimposed on the inherited structural framework.

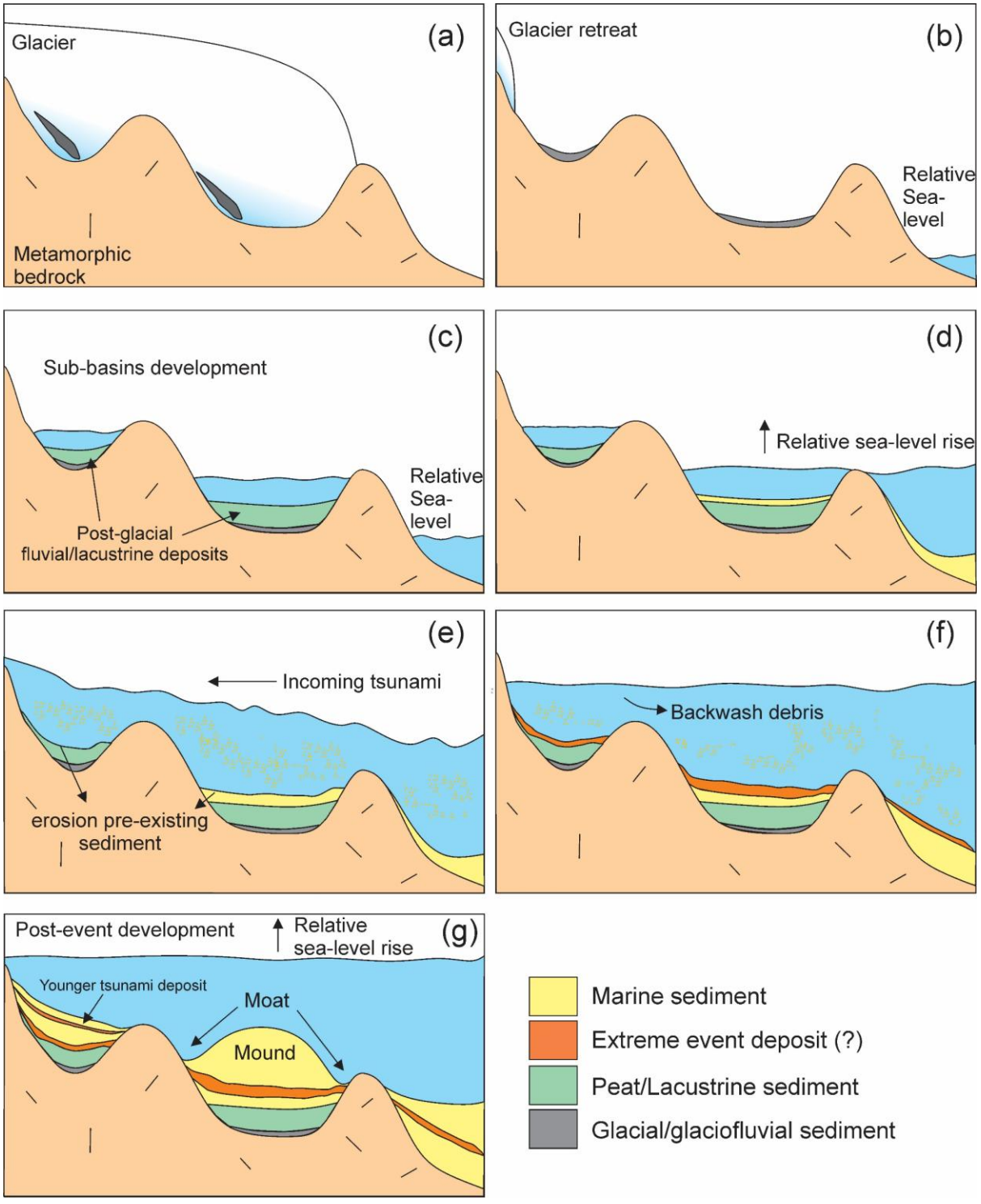

Figure 12. Schematic illustration of the proposed post-glacial stratigraphic evolution of the shallow offshore zone in Shetland Islands, showing the progressive transition from glacial conditions to fully marine sedimentation and the emplacement of extreme-wave deposits. (a) Glacial stage, with ice occupying structurally controlled depressions carved into metamorphic bedrock. (b) Glacier retreat and initial exposure of overdeepened basins, locally mantled by glacial and glaciofluvial sediments. (c) Early post-glacial phase characterized by the development of isolated sub-basins, infilled by low-energy lacustrine, estuarine, or very sheltered marine sediments. (d) Marine transgression during the early Holocene, leading to increased basin connectivity and the onset of marine sedimentation with progressively stronger hydrodynamic influence. (e) Emplacement of an extreme-wave event (tsunami), generating high-energy flow across the basin and erosion of pre-existing marine sediments. (f) Deposition of a laterally extensive, shell-rich event layer during the waning-flow and backwash phase, with reworked sediment transported and ponded within basin depressions. (g) Post-event evolution marked by continued sea-level rise and the development of laterally extensive, current-dominated marine sands forming mounded drift geometries that cap the sedimentary succession.

5.3 Event stratigraphy and extreme-wave deposits

5.3.1 Regional identification and correlation of tsunami deposits

Offshore basins may provide favorable conditions for the preservation of tsunami deposits thanks to reduced post-depositional reworking, continuous background sedimentation, and accommodation space created by basin morphology (Fig 12e, f). In seismic data, such deposits are typically expressed as laterally continuous, high-amplitude reflections or as seismic units with very distinct contacts and anomalous internal facies (Costa et al., 2021b; Feist et al., 2023; 2025)

In the Shetland region, the only documented occurrence of offshore tsunami deposits is in Fetlar Basin, where Earland et al. (2024) identified a laterally extensive, shell-rich event layer, whose radiocarbon age overlaps with that of the Storegga tsunami. This deposit is characterized by erosional basal contacts and poor sorting. Comparable characteristics are observed in this study, in which a laterally traceable high-energy event deposit was identified at all three sites. This deposit is consistently distinguished from background marine sedimentation by a sharp basal contact, poor sorting, shell-rich and locally gravelly composition, and distinctive high-amplitude seismic reflections.

The chronological framework based on radiocarbon ages is consistent with deposition during the time window of the Storegga Slide tsunami. This temporal agreement, combined with the sedimentological and seismic characteristics of the deposit, supports its interpretation as an event layer caused by the Storegga Slide tsunami. In addition to the offshore evidence at Fetlar Basin (Earland et al., 2024), this event layer is now also traced in shallower marine settings of Dury Voe, Colgrave Sound/Basta Voe, and Yell Sound. Notably, the tsunami deposit reaches its greatest thickness and most continuous preservation in Yell Sound, which may reflect its more direct exposure to tsunami waves propagating from the northern Storegga source area. The deposit can further be linked to well-documented onshore Storegga tsunami sediments across Shetland, preserved as sand sheets and gravel layers interbedded with peat and lacustrine sediments (Dawson et al., 2020; Bondevik et al., 2005), although no onshore Storegga tsunami deposits have yet been reported from the region of Dury Voe and Colgrave Sound/Basta Voe. The results of this study demonstrate the near-continuous preservation of the Storegga tsunami deposit from deep offshore basins through shallow-marine voes and into subaerial coastal environments.

A younger event deposit dated to ca. 1500 cal BP is identified in Dury Voe and correlates with a historically and stratigraphically recognized late Holocene tsunami recorded onshore in the region of Dury Voe and Basta Voe (Bondevik et al., 2005; Dawson et al., 2006). In contrast, no offshore equivalent is yet identified for the ca. 5500 cal BP tsunami reported from the Garth area south of Dury Voe (Bondevik et al., 2005). This absence is more likely related to a lower event magnitude, to the event having had only a local impact or to poor preservation, rather than limited sediment availability, with deposits either not formed or not distinguishable from background sedimentation.

6 Conclusion

This study demonstrates that shallow offshore voes and embayments of the Shetland Islands preserve a regionally coherent record of post-glacial sedimentary evolution, despite pronounced differences in basin geometry, water depth, and hydrodynamic exposure. Sedimentation in Dury Voe, Colgrave Sound/Basta Voe, and Yell Sound is strongly controlled by inherited bedrock morphology shaped by the pre-existing tectonic fabric and selective glacial erosion, resulting in preferential infilling of overdeepened sub-basins while intervening bedrock highs remain sediment-starved. Across all basins, the stratigraphic succession records a consistent four-stage evolution from a pre-marine glacial or glaciofluvial substrate, through low-energy early post-glacial infill deposited under restricted

conditions, into a transgressive phase marked by increasing marine influence, and finally to sand-dominated, current-influenced sedimentation forming laterally extensive mounded drift geometries. High-amplitude seismic units with sharp erosional bases and shell-rich, poorly sorted lithologies record regionally significant extreme-wave events. A prominent event deposit dated to ca. 8150 cal BP is correlated with the Storegga Slide tsunami and can be traced from deep offshore basins into shallow voes and nearshore settings. A younger Late Holocene event, originally dated to ca. 1500 cal BP based on onshore peat records (Bondevik et al., 2005), is also identified in the study area. However, the preservation of the event deposit differs markedly between offshore and onshore environments. In Dury Voe, this ca. 1500 cal BP event is clearly identified in the offshore record but has no confirmed onshore equivalent. In contrast, in Basta Voe the same event is well preserved in onshore peat sequences but is not clearly recorded offshore. This spatial variability indicates that offshore and onshore records are complementary rather than redundant, with each environment selectively preserving tsunami deposits. Consequently, shallow offshore basins provide critical additional information that is not consistently captured in onshore archives alone. The preservation of these event deposits across a wide range of palaeo-water depths highlights the importance of shallow offshore basins as archives of extreme-wave processes and early Holocene relative sea-level change. Overall, this work bridges the gap between deep offshore and onshore records and establishes shallow voes and embayments as key, yet underexplored, components of post-glacial stratigraphic frameworks and coastal hazard reconstructions in glaciated, tectonically complex settings.

Acknowledgement and Funding

This research was conducted within the NORSEAT project ("Storegga and beyond – North Sea tsunami deposits offshore Shetland Islands", grant agreement RV/21/NORSEAT), funded by the Belgian Science Policy Office (BELSPO). We further thank to the Flanders Marine Institute (VLIZ) for supporting the Vibrocoring operations. We also thank to the Poznań Radiocarbon Laboratory Polan regarding the Radiocarbon Analysis. Finally, we would like to thank all the crew and scientific party of RV Belgica cruises 2022/31 and 2023/16 for their assistance during offshore data acquisition and sediment sampling.

Author contributions

RAN: conceptualization, methodology, investigation, formal analysis, visualization, data curation, writing-original draft.
MVD: conceptualization, investigation, methodology, supervision, project administration, writing-original draft.
PC: investigation, methodology, data curation, writing-review and editing.
ME: investigation, methodology, data curation, writing-review and editing.
SD: investigation, writing-review and editing.
JS: investigation, writing-review and editing.
TG: investigation, writing-review and editing.
VH: funding acquisition, project administration, writing-review and editing.
MDB: conceptualization, methodology, funding acquisition, project administration, supervision, writing-original draft.

Declaration of competing interest

The authors declare no competing financial or personal relationship interests.

AI statement

During the preparation of this work, the authors used ChatGPT (OpenAI) to assist with language improvement, text structuring, and editing. After using this tool, the authors reviewed and edited the content as needed and take full responsibility for the content of the published article.

References

Balascio, N.L., Zhang, Z., Bradley, R.S., Perren, B.B., Dahl, S.O., Bakke, J., 2011. A multi-proxy approach to assessing isolation basin stratigraphy from the Lofoten Islands, Norway. Quat. Res. 75, 288–300. https://doi.org/10.1016/j.yqres.2010.08.012

Best, A.I., Sothcott, J., McCann, C., 2007. A laboratory study of seismic velocity and attenuation anisotropy in near-surface sedimentary rocks. Geophys. Prospect. 55, 609–625. https://doi.org/10.1111/j.1365-2478.2007.00642.x

Bianchi, T., Arndt, S., Austin, W., Benn, D., Bertrand, S., Cui, X., Faust, J., Koziorowska-Makuch, K., Moy, C., Savage, C., Smeaton, C., Smith, R., Syvitski, J., 2020. Fjords as Aquatic Critical Zones (ACZs). Earth Sci. Rev. 203, 103145. https://doi.org/10.1016/j.earscirev.2020.103145

Bondevik, S., Mangerud, J., Dawson, S., Dawson, A., Lohne, Ø., 2003. Record-breaking height for 8000-year-old tsunami in the North Atlantic. Eos, Transactions American Geophysical Union 84, 289–293. https://doi.org/10.1029/2003EO310001

Bondevik, S., Mangerud, J., Dawson, S., Dawson, A., Lohne, Ø., 2005. Evidence for three North Sea tsunamis at the Shetland Islands between 8000 and 1500 years ago. Quat. Sci. Rev. 24, 1757–1775. https://doi.org/10.1016/j.quascirev.2004.10.018

Bondevik, S., Stormo, S.K., Skjerdal, G., 2012. Green mosses date the Storegga tsunami to the chilliest decades of the 8.2 ka cold event. Quat. Sci. Rev. 45, 1–6. https://doi.org/10.1016/j.quascirev.2012.04.020

Bradwell, T., Small, D., Fabel, D., Clark, C.D., Chiverrell, R.C., Saher, M.H., Dove, D., Callard, S.L., Burke, M.J., Moreton, S.G., Medialdea, A., Bateman, M.D., Roberts, D.H., Golledge, N.R., Finlayson, A., Morgan, S., Ó Cofaigh, C., 2019. Pattern, style and timing of British–Irish Ice Sheet retreat: Shetland and northern North Sea sector. J. Quat. Sci. 36, 681–722. https://doi.org/10.1002/jqs.3163

Bradwell, T., Stoker, M.S., 2015. Submarine sediment and landform record of a palaeo-ice stream within the British-Irish ice sheet. Boreas 44, 255–276. https://doi.org/10.1111/bor.12111

Bradwell, T., Stoker, M.S., 2016. Glacial sediment and landform record offshore NW Scotland: a fjord–shelf–slope transect through a Late Quaternary mid-latitude ice-stream system. Geological Society, London, Memoirs 46, 421–428. https://doi.org/10.1144/M46.152

British Geological Survey, 1991. Quaternary Map of the UK Continental Shelf: Sheet 58N–04W.

Bronk Ramsey, C., 1995. Radiocarbon Calibration and Analysis of Stratigraphy: The OxCal Program. Radiocarbon 37(2), 425–430. https://doi.org/10.1017/S0033822200030903

Burschil, T., Tanner, D., Reitner, J., Buness, H., Gabriel, G., 2019. Unravelling the shape and stratigraphy of a glacially-overdeepened valley with reflection seismic: the Lienz Basin (Austria). Swiss J. Geosci. 112, 341–355. https://doi.org/10.1007/s00015-019-00339-0

Chotiros, N.P., 2002. Acoustic modeling of sandy ocean sediments. Proceedings of the 2002 International Symposium on Underwater Technology (Cat. No.02EX556), Tokyo, Japan, 2002, pp. 231-236. https://doi.org/10.1109/UT.2002.1002431

Clark, C.D., Ely, J.C., Hindmarsh, R.C.A., Bradley, S., Ignéczi, A., Fabel, D., Ó Cofaigh, C., Chiverrell, R.C., Scourse, J., Benetti, S., Bradwell, T., Evans, D.J.A., Roberts, D.H., Burke, M., Callard, S.L., Medialdea, A., Saher, M., Small, D., Smedley, R.K., Gasson, E., Gregoire, L., Gandy, N., Hughes, A.L.C., Ballantyne, C., Bateman, M.D., Bigg, G.R., Doole, J., Dove, D., Duller, G.A.T., Jenkins, G.T.H., Livingstone, S.L., McCarron, S., Moreton, S., Pollard, D., Praeg, D., Sejrup, H.P., Van Landeghem, K.J.J., Wilson, P., 2022. Growth and retreat of the last British–Irish Ice Sheet, 31 000 to 15 000 years ago: the BRITICE-CHRONO reconstruction. Boreas 51, 699–758. https://doi.org/10.1111/bor.12594

Costa, P.J.M., Andrade, C., 2020. Tsunami deposits: Present knowledge and future challenges. Sedimentology 67, 1189–1206. https://doi.org/10.1111/sed.12724

Costa, P.J.M., Dawson, S., Engel, M., Nahar, R., Scheder, J., Goovaerts, T., De Rycker, K., Matossian, A., Bastos, A., Caetano, J., Carvalho, V., Haelters, J., 2022. RV BELGICA Cruise 2022/31 Report.

Costa, P.J.M., Dawson, S., Ramalho, R.S., Engel, M., Dourado, F., Bosnic, I., Andrade, C., 2021a. A review on onshore tsunami deposits along the Atlantic coasts. Earth Sci. Rev. 212, 103441. https://doi.org/10.1016/j.earscirev.2020.103441

Costa, P.J.M., Feist, L., Dawson, A.G., Stewart, I., Reicherter, K., Andrade, C., 2021b. An overview on offshore tsunami deposits, in: Shiki, T., Tsuji, Y., Yamazaki, T., Nanayama, F. (Eds.), Tsunamiites (Second Edition). Elsevier, pp. 183–192. https://doi.org/10.1016/B978-0-12-823939-1.00011-2

Dawson, A., Dawson, S., Bondevik, S., Costa, P.J.M., Hill, J., Stewart, I., 2020. Reconciling Storegga tsunami sedimentation patterns with modelled wave heights: A discussion from the Shetland Isles field laboratory. Sedimentology 67, 1344–1353. https://doi.org/10.1111/sed.12643

Dawson, A.G., Dawson, S., Bondevik, S., 2006. A Late Holocene Tsunami at Basta Voe, Yell, Shetland Isles. Scottish Geographical Journal 122(2), 100–108. https://doi.org/10.1080/00369220600917404

Dawson, A.G., Stewart, I., 2007. Tsunami deposits in the geological record. Sediment. Geol. 200, 166–183. https://doi.org/10.1016/j.sedgeo.2007.01.002

Earland, J.L., Scourse, J.D., Ehmen, T., Kender, S., Ascough, P., 2024. Identification of the Storegga event offshore Shetland. Mar. Geol. 474, 107334. https://doi.org/10.1016/j.margeo.2024.107334

Engel, M., Hess, K., Dawson, S., Patel, T., Koutsodendris, A., Vakhrameeva, P., Klemt, E., Kempf, P., Schön, I., Heyvaert, V.M.A., 2023. Sedimentary evidence of the Late Holocene tsunami in the Shetland Islands (UK) at Loch Flugarth, northern Mainland. Boreas 53, 27–41. https://doi.org/10.1111/bor.12635

Farr, T.G., Rosen, P.A., Caro, E., Crippen, R., Duren, R., Hensley, S., Kobrick, M., Paller, M., Rodriguez, E., Roth, L., Seal, D., Shaffer, S., Shimada, J., Umland, J., Werner, M., Oskin, M., Burbank, D., Alsdorf, D.E., 2007. The shuttle radar topography mission. Reviews of Geophysics 45, 63–96. https://doi.org/10.1029/2005RG000183

Farrow, G., Allen, N., Akpan, E., 1984. Bioclastic carbonate sedimentation on a high-latitude, tide-dominated shelf; Northeast Orkney Islands, Scotland. Journal of Sedimentary Research 54, 373–393. https://doi.org/10.1306/212f8422-2b24-11d7-8648000102c1865d

Feist, L., Costa, P.J.M., Bellanova, P., Bosnic, I., Santisteban, J.I., Andrade, C., Brückner, H., Duarte, J.F., Kuhlmann, J., Schwarzbauer, J., Vött, A., Reicherter, K., 2023. Holocene offshore tsunami archive – Tsunami deposits on the Algarve shelf (Portugal). Sediment. Geol. 448, 106369. https://doi.org/10.1016/j.sedgeo.2023.106369

Feist, L., Costa, P.J.M., Santisteban, J.I., Albers, S., Bellanova, P., Bosnic, I., De Batist, M., Duarte, J.F., Rodrigues, A., Reicherter, K., 2025. Shallow seismic stratigraphy of the southwestern Algarve shelf (Portugal) and characteristics of offshore tsunami deposits. Mar. Geol. 480, 107463. https://doi.org/10.1016/j.margeo.2024.107463

Flinn, D., 2007. The Dalradian rocks of Shetland and their implications for the plate tectonics of the northern Iapetus. Scottish Journal of Geology 43, 125–142. https://doi.org/10.1144/sjg43020125

Forbes, D., Shaw, J., Eddy, B., 1993. Late Quaternary sedimentation and the postglacial sea-level minimum in Port au Port Bay and vicinity, west Newfoundland. Atlantic Geoscience 29, 1–26. https://doi.org/10.4138/1986

Gao, S., Collins, M.B., 2014. Holocene sedimentary systems on continental shelves. Mar. Geol. 352, 268–294. https://doi.org/10.1016/j.margeo.2014.03.021

GEBCO Compilation Group, 2025. The GEBCO_2025 Grid – a continuous terrain model of the global oceans and land at 15 arc-second intervals. NERC EDS British Oceanographic Data Centre NOC. https://doi.org/doi:10.5285/37c52e96-24ea-67ce-e063-7086abc05f29

Goslar, T., Czernik, J., Goslar, E., 2004. Low-energy ^{14}C AMS in Poznań Radiocarbon Laboratory, Poland, in: Nuclear Instruments and Methods in Physics Research, Section B: Beam Interactions with Materials and Atoms. pp. 5–11. https://doi.org/10.1016/j.nimb.2004.04.005

Hall, A.M., Ebert, K., Kleman, J., Nesje, A., Ottesen, D., 2013. Selective glacial erosion on the Norwegian passive margin. Geology 41, 1203–1206. https://doi.org/10.1130/G34806.1

Hall, A.M., Hansom, J.D., Gordon, J.E., 2021. Shetland, in: Ballantyne Colin K. and Gordon, J.E. (Ed.), Landscapes and Landforms of Scotland. Springer International Publishing, Cham, pp. 135–150. https://doi.org/10.1007/978-3-030-71246-4_7

Hamilton, E.L., 1980. Geoacoustic modeling of the sea floor. Journal of the Acoustical Society of America 68, 1313–1340. https://doi.org/10.1121/1.385100

Hayward, Peter J., and John S. Ryland (eds), Handbook of the Marine Fauna of North-West Europe, 2nd edn (Oxford, 2017; online edn, Oxford Academic, 20 Apr. 2017), https://doi.org/10.1093/acprof:oso/9780199549443.001.0001

Heaton, T.J., Köhler, P., Butzin, M., Bard, E., Reimer, R.W., Austin, W.E.N., Bronk Ramsey, C., Grootes, P.M., Hughen, K.A., Kromer, B., Reimer, P.J., Adkins, J., Burke, A., Cook, M.S., Olsen, J., Skinner, L.C., 2020. Marine20 - The Marine Radiocarbon Age Calibration Curve (0-55,000 cal BP). Radiocarbon 62, 779–820. https://doi.org/10.1017/RDC.2020.68

Hess, K., Engel, M., Patel, T., Vakhrameeva, P., Koutsodendris, A., Klemt, E., Hansteen, T.H., Kempf, P., Dawson, S., Schön, I., Heyvaert, V.M.A., 2024. A 1500-year record of North Atlantic storm

flooding from lacustrine sediments, Shetland Islands (UK). J. Quat. Sci. 39, 37–53. https://doi.org/10.1002/jqs.3568

Hodgson, D. M., Browning, J. V., Miller, K. G., Hesselbo, S. P., Poyatos-Moré, M., Mountain, G. S., & Proust, J. N. (2017). Sedimentology, stratigraphic context, and implications of Miocene intrashelf bottomset deposits, offshore New Jersey. Geosphere, 14(1), 95–114. https://doi.org/10.1130/GES01530.1

Hogan, K.A., Jakobsson, M., Mayer, L., Reilly, B.T., Jennings, A.E., Stoner, J.S., Nielsen, T., Andresen, K.J., Nørmark, E., Heirman, K.A., Kamla, E., Jerram, K., Stranne, C., Mix, A., 2020. Glacial sedimentation, fluxes and erosion rates associated with ice retreat in Petermann Fjord and Nares Strait, north-west Greenland. Cryosphere 14, 261–286. https://doi.org/10.5194/tc-14-261-2020

Howe, J.A., Stoker, M.S., Stow, D.A. V, Akhurst, M.C., 2002. Sediment drifts and contourite sedimentation in the northeastern Rockall Trough and Faroe-Shetland Channel, North Atlantic Ocean. Geological Society, London, Memoirs 22, 65–72. https://doi.org/10.1144/GSL.MEM.2002.022.01.06

Husum, K., Howe, J.A., Baltzer, A., Forwick, M., Jensen, M., Jernas, P., Korsun, S., Miettinen, A., Mohan, R., Morigi, C., Myhre, P.I., Prins, M.A., Skirbekk, K., Sternal, B., Boos, M., Dijkstra, N., Troelstra, S., 2019. The marine sedimentary environments of Kongsfjorden, Svalbard: An archive of polar environmental change. Polar Res. 38, 3388. https://doi.org/10.33265/polar.v38.3380

Knutz, P.C., Cartwright, J., 2003. Seismic stratigraphy of the West Shetland Drift: Implications for late Neogene paleocirculation in the Faeroe-Shetland gateway. Paleoceanography 18, 1093. https://doi.org/10.1029/2002PA000786

Lo Giudice Cappelli, E., Clarke, J., Smeaton, C., Davidson, K., Austin, W., 2019. Organic-carbon-rich sediments: benthic foraminifera as bio-indicators of depositional environments. Biogeosciences 16, 4183–4199. https://doi.org/10.5194/bg-16-4183-2019

Lo Giudice Cappelli, E., Austin, W.E.N., 2020. Marine Bivalve Feeding Strategies and Radiocarbon Ages in Northeast Atlantic Coastal Waters. Radiocarbon, 62, 107-125. https://doi.org/10.1017/RDC.2019.68

López-Jamar, E., González, G., Mejuto, J., 1987. Ecology, growth and production of *Thyasira flexuosa* (Bivalvia, Lucinacea) from Ría de La Coruña, North-West Spain. *Ophelia* 27 (2): 111–26. https://doi.org/10.1080/00785236.1987.10422015

Marine Scotland, 2019. National Marine Plan Interactive (NMPi). URL https://marine.gov.scot (accessed 8.17.25).

Morton, R.A., Gelfenbaum, G., Jaffe, B.E., 2007. Physical criteria for distinguishing sandy tsunami and storm deposits using modern examples. Sediment. Geol. 200, 184–207. https://doi.org/10.1016/j.sedgeo.2007.01.003

Mykura, W., 1976. The Geology of Shetland. HMSO for the British Geological Survey.

Mykura, W., Flinn, D., May, F., 1976. British Regional Geology – Orkney and Shetland. National Environment Research Council, Institute of Geological Sciences, Edinburgh.

Nichols, Gary., 2009. Sedimentology and stratigraphy. Wiley-Blackwell.

Nolf, F., Vandenberge, Q., 2012a: On an important collection of seashells from the Shetland Islands: part I. Neptunea 11(3), 1-30.

Nolf, F., Vandenberge, Q., 2012b: On an important collection of seashells from the Shetland Islands: part II. Neptunea 11(4), 1-30.

Ó Cofaigh, C., Hogan, K.A., Dowdeswell, J.A., Streuff, K.T., 2016. Stratified glacimarine basin-fills in West Greenland fjords. Geological Society, London, Memoirs 46, 99–100. https://doi.org/https://doi.org/10.1144/M46.83

Oliver, P.G., Holmes, A.M., Killeen, I.J., Turner, J.A., 2016. Marine Bivalve Shells of the British Isles. URL http://naturalhistory.museumwales.ac.uk/britishbivalves (accessed 3.30.26).

Phillips, W.M., Hall, A.M., Ballantyne, C.K., Binnie, S.A., Kubik, P.W., Freeman, S.P.H.T., 2008. Extent of the last ice sheet in northern Scotland tested with cosmogenic ^{10}Be exposure ages. J. Quat. Sci. 23(2), 101–107. https://doi.org/10.1002/jqs.1161

Poiré, A., Lajeunesse, P., Normandeau, A., Francus, P., St-Onge, G., Nzekwe, O., 2018. Late-Quaternary glacial to postglacial sedimentation in three adjacent fjord-lakes of the Québec North Shore (eastern Canadian Shield). Quat. Sci. Rev. 186, 91–110. https://doi.org/10.1016/j.quascirev.2018.02.013

Rebesco, M., Hernández-Molina, F.J., Van Rooij, D., Wåhlin, A., 2014. Contourites and associated sediments controlled by deep-water circulation processes: State-of-the-art and future considerations. Mar. Geol. 352, 111–154. https://doi.org/10.1016/j.margeo.2014.03.011

Reimer, P.J., Austin, W.E.N., Bard, E., Bayliss, A., Blackwell, P.G., Bronk Ramsey, C., Butzin, M., Cheng, H., Edwards, R.L., Friedrich, M., Grootes, P.M., Guilderson, T.P., Hajdas, I., Heaton, T.J., Hogg, A.G., Hughen, K.A., Kromer, B., Manning, S.W., Muscheler, R., Palmer, J.G., Pearson, C., Van Der Plicht, J., Reimer, R.W., Richards, D.A., Scott, E.M., Southon, J.R., Turney, C.S.M., Wacker, L., Adolphi, F., Büntgen, U., Capano, M., Fahrni, S.M., Fogtmann-Schulz, A., Friedrich, R., Köhler, P., Kudsk, S., Miyake, F., Olsen, J., Reinig, F., Sakamoto, M., Sookdeo, A., Talamo, S., 2020. The IntCal20 Northern Hemisphere Radiocarbon Age Calibration Curve (0-55 cal kBP). Radiocarbon 62, 725–757. https://doi.org/10.1017/RDC.2020.41

Reimer, P.J., Reimer, R.W., 2001. A marine reservoir correction database and on-line interface. Radiocarbon 43, 461–463. https://doi.org/10.1017/S0033822200038339

Hall, A.M., Hansom, J.D., Gordon, J.E., 2021. Shetland. In: Ballantyne, C.K., Gordon, J.E. (eds) Landscapes and Landforms of Scotland. World Geomorphological Landscapes. Springer, Cham. https://doi.org/10.1007/978-3-030-71246-4_7

Sharrocks, P.D., Peakall, J., Hodgson, D.M., Barlow, N.L.M., 2025. Tsunami versus storms: Diagnostic sedimentary criteria in coastal lakes, lagoons and sinkhole deposits. Earth Sci. Rev. 271, 105277. https://doi.org/10.1016/j.earscirev.2025.105277

Shennan, I., Horton, B., 2002. Holocene land- and sea-level changes in Great Britain. J. Quat. Sci. 17, 511–526. https://doi.org/10.1002/jqs.710

Shetland Islands Council, 2023. Shetland statistics: Economy. URL https://www.shetland.gov.uk/shetland-statistics/economy/2 (accessed 3.13.26).

Smith, D.E., Barlow, N.L.M., Bradley, S.L., Firth, C.R., Hall, A.M., Jordan, J.T., Long, D., 2019. Quaternary sea level change in Scotland. Earth Environ. Sci. Trans. R. Soc. Edinb. 110, 219–256. https://doi.org/10.1017/S1755691017000469

Stein, A.M., 1988. Basement controls upon basin development in the Caledonian foreland, NW Scotland. Basin Research 1, 107–119. https://doi.org/10.1111/j.1365-2117.1988.tb00008.x

Stockamp, J., Bishop, P., Li, Z., Petrie, E., Hansom, J., Rennie, A., 2015. State-of-the-art in studies of glacial isostatic adjustment for the British Isles: a literature review. Earth Environ. Sci. Trans. R. Soc. Edinb. 106, 145–170. https://doi.org/10.1017/s1755691016000074

Syvitski, J.P.M., Burrell, D.C., Skei, J.M., 1987. Fjords and Their Study, in: Syvitski, J.P.M., Burrell, D.C., Skei, J.M. (Eds.), Fjords. Springer New York, pp. 3–17. https://doi.org/10.1007/978-1-4612-4632-9

Syvitski, J.P.M., Shaw, J., 1995. Sediment transport and deposition in glaciated fjords: a review. Oceanography and Marine Biology: An Annual Review 33, 1–59.

Trottier, A., Lajeunesse, P., Gagnon-Poiré, A., Francus, P., 2020. Morphological signatures of deglaciation and postglacial sedimentary processes in a deep fjord-lake (Grand Lake, Labrador). Earth Surf. Process. Landf. 45, 928–947. https://doi.org/10.1002/esp.4786

Van Daele, M., Costa, P.J.M., Engel, M., Nahar, R., Lisson, K., Goovaerts, T., Bertels, R., Meyvis, B., Teixeira, M., Dourado, F., Cavadas, H., Hess, K., Peffeköver, A., Blomme, W., Vermaut, J., Weber Mesquita, Y., Stempels Bautista, C., 2023. Belgica 2023/16 Cruise Report.

Wahl, T., Haigh, I., Albrecht, F., Dillingh, D., Jensen, J., Nicholls, R., Weisse, R., Woodworth, P.L., Wöppelmann, G., 2013. Observed mean sea level changes around the North Sea coastline from 1800 to present. Earth Sci. Rev. 124, 51–67. https://doi.org/10.1016/j.earscirev.2013.05.003

Watts, L.M., Holdsworth, R.E., Sleight, J.A., Strachan, R.A., Smith, S.A.F., 2007. The movement history and fault rock evolution of a reactivated crustal-scale strike-slip fault: The Walls Boundary Fault Zone, Shetland. J. Geol. Soc. London. 164, 1037–1058. https://doi.org/10.1144/0016-76492006-156

Wilckens, H., Eggenhuisen, J.T., Adema, P.H., Hernández-Molina, F.J., Jacinto, R.S., Miramontes, E., 2023. Secondary flow in contour currents controls the formation of moat-drift contourite systems. Commun. Earth Environ. 4, 316. https://doi.org/10.1038/s43247-023-00978-0

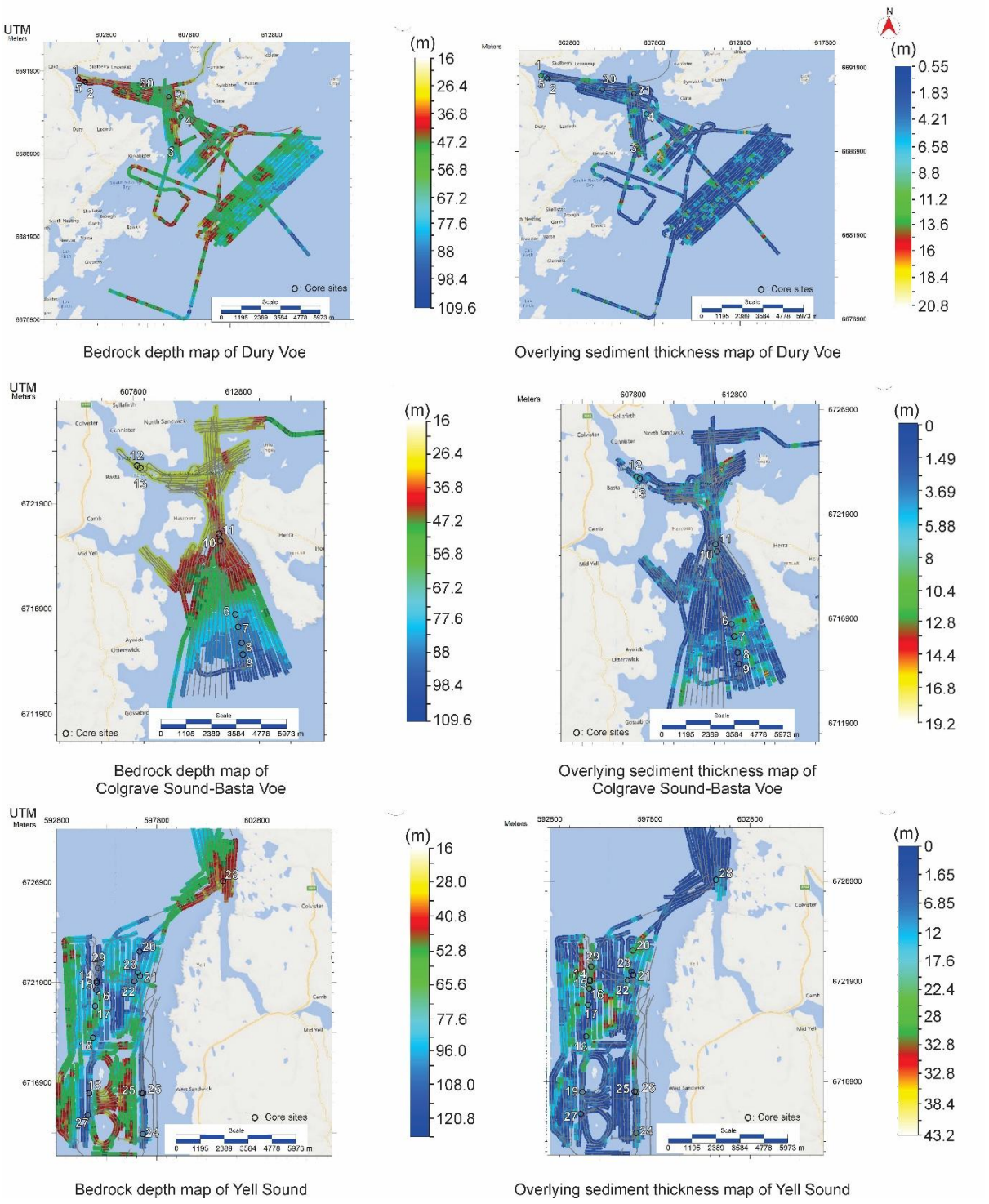

Supplementary Figure S1. Depth-to-bedrock and overlying sediment thickness (isopach) maps derived from seismic interpretation in the three investigated basins offshore Shetland. Upper panels show Dury Voe, middle panels show Colgrave Sound–Basta Voe, and lower panels show Yell Sound. Left panels present depth-to-bedrock maps, whereas right panels illustrate the thickness distribution of the overlying sedimentary infill. Depths and sediment thicknesses were calculated from two-way travel time (TWT) data using a constant acoustic velocity of 1600 m/s. The maps demonstrate that early accommodation space was strongly controlled by inherited bedrock morphology, with sediment preferentially accumulating within overdeepened depressions. In contrast, the distribution of younger marine sediments locally forms elongated sediment bodies and drift-like accumulations that are partly

decoupled from basement relief, reflecting enhanced sediment redistribution by bottom currents following marine transgression. Coordinate system: UTM Zone 30N (WGS84).